ACS APPLIED MATERIALS & INTERFACES

Research Article

www.acsami.org

# Screen-Printable and Flexible $RuO_2$ Nanoparticle-Decorated PEDOT:PSS/Graphene Nanocomposite with Enhanced Electrical and Electrochemical Performances for High-Capacity Supercapacitor

Sunghun Cho,[†] Minkyu Kim,[‡] and Jyongsik Jang*[,†,‡]

[†]Program of Chemical Convergence for Energy and Environment (C2E2) and [‡]School of Chemical and Biological Engineering, College of Engineering, Seoul National University, Shinlimdong 56-1, Seoul 151-742, Korea

Supporting Information

**ABSTRACT:** This work describes a ternary screen-printed electrode system, composed of aqueous poly(3,4-ethylenedioxythiophene):poly(4-styrenesulfonic acid) (PEDOT:PSS), graphene, and hydrous ruthenium(IV) oxide ($RuO_2$) nanoparticles for use in high-performance electrochemical capacitors. As a polymeric binder, PSS allows stable dispersion of graphene and hydrous $RuO_2$ nanoparticles (NPs) in an aqueous PEDOT:PSS system through electrostatic stabilization, ensuring better utilization of the three components. Additional PSS molecules were added to optimize the solution viscosity to obtain screen-printed electrodes. The effects of graphene and hydrous $RuO_2$ NPs on the electrical and electrochemical properties of PEDOT:PSS were systematically investigated. The graphene sheets greatly enhanced the charge-transport properties, such as the doping level and conjugation length, through strong $\pi-\pi$ stacking interactions with the PEDOT structure. The hydrous $RuO_2$ NPs anchored to the PEDOT:PSS/graphene surfaces facilitated redox reactions with the surrounding electrolyte, and significantly enhanced the specific capacitance of the electrode materials. The resulting $RuO_2$/PEDOT:PSS/graphene electrode with a thickness of ~5 $\mu$m exhibited high conductivity (1570 S $cm^{-1}$), a large specific capacitance (820 F $g^{-1}$), and good cycling stability (81.5% after 1000 cycles).

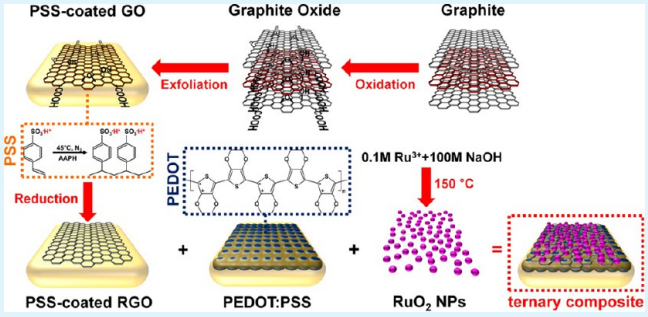


**KEYWORDS:** *poly(3,4-ethylenedioxythiophene), poly(4-styrenesulfonic acid), graphene, ruthenium oxide, screen-printing*

## INTRODUCTION

Polymeric acids, such as poly(4-styrenesulfonic acid) (PSS),[1−9] poly(vinylsulfonic acid) (PVS),[10] and poly(acrylic acid) (PAA),[11] have attracted great interest due to their simple film formation and tunable electrical conductivity. In particular, poly(3,4-ethylenedioxythiophene):poly(4-styrenesulfonic acid) (PEDOT:PSS) has been widely utilized as an electrode material in organic photovoltaics (OPVs),[3−5,12−18] dye-sensitized solar cells (DSSCs),[19−22] organic light-emitting diodes (OLEDs),[23] and sensors[24,25] due to its numerous advantages including a small band gap (1.6−1.7 eV), low redox potential, good optical properties, and high processability from aqueous solution.[1−7,16−21] In these devices, the conductivity of PEDOT:PSS is an important factor with regard to device performance.[16−18] Various organic compounds with high dielectric constants, such as dimethyl sulfoxide (DMSO), ethylene glycol (EG), tetrahydrofuran (THF), sorbitol, *N*-methylpyrrolidone (NMP), isopropanol (IPA), and *N*,*N*-dimethyl formaldehyde (DMF), increase the conductivity of PEDOT:PSS by several orders of magnitude (up to ~$10^3$ S $cm^{-1}$) by reducing the ionic interactions between positively charged PEDOT and negatively charged PSS.[2−5,15−21,26−28,78,79] Due to their high conductivity, PEDOT:PSS thin films have been considered for use as the cathode material in electrochemical capacitors.[29−34] But despite their high conductivity, conducting polymers, including PEDOT:PSS, usually suffer from a low capacitance because only a fractional number of electrons are obtainable from the monomer units of the polymer.[35]

Formation of conducting thin films with morphological homogeneity and dimensional stability has become a key issue for improving the performances of electronic devices.[3,6,8,9,36,37] Spin-coating provides a facile means to produce thin films from soluble conducting polymers. In the spin-coating method, the film thickness of conducting polymers is modified by adjusting the concentration of solution and the rotating rate of the spin-coater.[6,52] However, the spin-coating method does not support the partial coating of substrate or creation of specific patterns on the substrate. The inkjet printing method, a type of computer printing, can create specific patterns on large-scale substrates by propelling droplets of inks in the cartridge.[8] Despite its advantage, the cartridge used in inkjet printing is usually blocked and damaged by ink materials unless the

Received: January 21, 2015
Accepted: April 28, 2015
Published: May 8, 2015




DOI: 10.1021/acsami.5b00657
ACS Appl. Mater. Interfaces 2015, 7, 10213−10227

**Scheme 1. Overall Procedure for Fabricating $RuO_2$/PEDOT:PSS/Graphene Screen-Printed Electrode and Digital Camera Image of Screen-Printed Electrode**

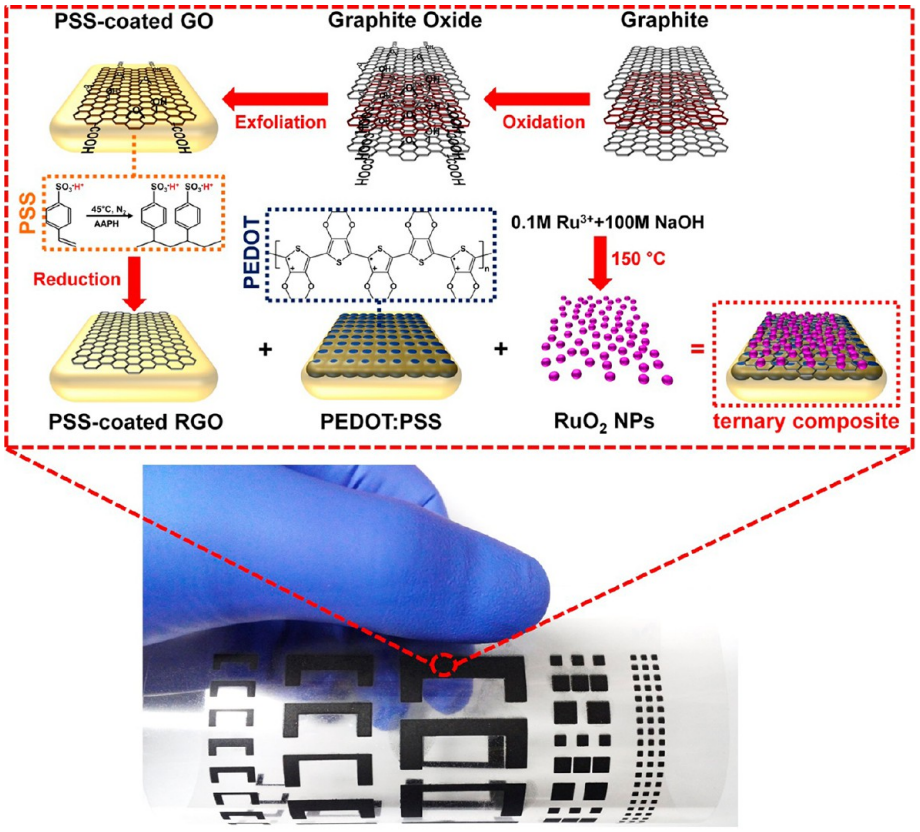


cartridge is washed within 1 day; thus, the ink materials for inkjet printing should be water-soluble solution with low viscosity. Moreover, ink materials used in the inkjet printing method are not reusable; therefore, large amounts of inks are wasted during the process. Recently, screen-printing has provided a simple, effective way to obtain defined patterns of conducting materials with various shapes and sizes.[9,36,37] Compared with the spin-coating and inkjet printing methods, the screen-printing method provides the following advantages. (1) In the screen-printing method, the conducting polymer solutions can be transferred onto both rigid and flexible substrates, such as poly(ethylene terephthalate) (PET), polycarbonate (PC), poly(methyl methacrylate) (PMMA), polyimide (PI), glass, and metals, through a screen mask that contains the specifically designed patterns. (2) Inks used in the screen-printing method are reproducible and reusable. (3) More importantly, the screen-printing method is a mass-producible and highly scalable system, which makes it suitable for many industrial and practical applications. In general, conducting inks for screen-printing require a relatively high viscosity ($\sim 10^3$ centipoise, cP) to achieve good adhesion between the patterns and the substrate. Despite the high conductivity of PEDOT:PSS, most PEDOT:PSS solutions usually have viscosities of less than $10^2$ cP to facilitate transparent thin-film formation.[37] As a water-dispersible polymeric binder, PSS possesses a high viscosity; this viscosity can be tuned by controlling the molecular weight or monomer concentration of PSS.[9] Moreover, PSS possesses sufficient sulfonate groups ($-SO_3^-$), which enable uniform anchoring and good dispersion of various materials through electrostatic repulsion interactions.[38,39] For this reason, PSS is a promising material for optimizing the viscosity of PEDOT:PSS solutions for screen-printing onto flexible plastic substrates. However, an excess of polymeric binders significantly lowers the conductivity of PEDOT:PSS-based electrodes due to their insulating properties.[40] Hence, the preparation of PEDOT:PSS inks for fabricating screen-printed electrodes having both high conductivity ($>10^3$ S $cm^{-1}$) and optimized viscosity ($>10^3$ cP) still poses a challenge.

Graphene, consisting of $sp^2$-hybrid carbon atoms with a honeycomb crystal structure, is a promising candidate for constructing conductive composites with various components, including conducting polymers and metals, due to its outstanding charge-transport properties, mechanical strength, and flexibility.[41,55−65,81−83] The PEDOT/graphene composite system has been widely used as an electrode material for electrochemical capacitors.[32−34,42−44] In PEDOT/graphene binary composites, the graphene sheets form strong $\pi-\pi$ stacking interactions with the thiophene rings of the PEDOT structure; this significantly enhances the charge-transport properties of the binary electrode.[38,45] Such $\pi-\pi$ stacking interactions become magnified when graphene is highly dispersed throughout the PEDOT solution. Thus, a homogeneous dispersion of reduced graphene in an aqueous phase is essential for improving the charge-transport properties of PEDOT:PSS. Several papers have reported the formation of a stable dispersion of reduced graphene by electrostatic repulsion interactions between the $-SO_3^-$ groups of PSS and graphene.[38,39] In addition, the solution viscosity of PEDOT:PSS/graphene may increase with the filler content. Accordingly, a PEDOT:PSS/graphene system with an optimal amount of graphene can induce a higher solution viscosity and


DOI: 10.1021/acsami.5b00657
ACS Appl. Mater. Interfaces 2015, 7, 10213−10227

enhanced charge-transport properties compared with pristine PEDOT:PSS.

Ruthenium(IV) oxide ($RuO_2$) nanoparticles (NPs), especially the hydrous and amorphous forms, offer great potential as a pseudocapacitor component due to their fascinating virtues (e.g., high capacitance, fast redox behavior, and good electrical conductivity).[29,30,46,47,77] Both PEDOT:PSS and graphene sheets provide functional groups that promote uniform dispersion of $RuO_2$ NPs. For this reason, $RuO_2$ NPs are promising for hybrid electrode systems consisting of PEDOT:PSS and graphene sheets. Thus, it is necessary to combine advantages of each component, such as rapid ion sorption/desorption of carbon materials and facile redox behaviors of pseudocapacitive materials, for construction of high-performance electrochemical capacitors.[55−77]

Herein, we report the preparation of water-dispersible $RuO_2$-decorated PEDOT:PSS/graphene-based screen-printing inks for use as electrode materials in high-performance electrochemical capacitors. To our knowledge, this is the first demonstration of a ternary electrode system consisting of PEDOT:PSS, graphene, and hydrous $RuO_2$ NPs in an aqueous phase; this electrode configuration, obtained by screen-printing, exhibited high electrical and electrochemical performance. The PSS binders were inserted into the PEDOT:PSS solution to optimize the viscosity of the PEDOT:PSS-based inks for screen-printing. The PSS prepared by low-temperature radical polymerization in an aqueous phase provided a higher viscosity and molecular weight compared with conventional, commercialized PSS. Thus, only small amounts of PSS (1/5 v/v vs distilled water) were required for sufficient PEDOT:PSS solution viscosity. In the presence of high-molecular-weight PSS, graphene (size 2−10 $\mu$m) and hydrous $RuO_2$ NPs (diameter ∼5 nm) were highly dispersible in the PEDOT:PSS solution through electrostatic stabilization.[29,30,38,39] $RuO_2$/PEDOT:PSS/graphene solutions were formed as patterned electrodes on flexible plastic substrates; the patterned electrodes had a uniform thickness of 5 $\mu$m. To identify the optimal amount of graphene for the PEDOT:PSS/graphene composite, the changes in conductivity and electrochemical activity as a function of graphene content were evaluated. The synergetic effects from PEDOT:PSS, graphene, and hydrous $RuO_2$ NPs on the morphological, charge-transport, and electrochemical properties were systematically investigated. The resulting $RuO_2$/PEDOT:PSS/graphene screen-printed electrode system exhibited significantly higher conductivity (1570 S $cm^{-1}$), a larger specific capacitance (820 F $g^{-1}$), and better cycling performance (81.5% after 1000 cycles) compared with PEDOT:PSS, making this system suitable for electrochemical capacitors.

## RESULTS AND DISCUSSION

**Structure of $RuO_2$/PEDOT:PSS/Graphene Nanocomposite.** Scheme 1 describes the fabrication methods of $RuO_2$/PEDOT:PSS/graphene nanocomposites. DMSO (5 wt %), which is known to enhance the conductivity of PEDOT:PSS by reducing the Coulomb interactions between PEDOT NPs and PSS molecules, was added to the PEDOT:PSS solution.[3−5] According to Hansen's equation, the DMSO/water cosolvent system provided appropriate hydrogen bonding ($\delta_h$) and polarity interaction ($\delta_p$) parameters, which are related to the stable dispersion of PSS-coated graphenes and hydrous $RuO_2$ NPs in the cosolvent system.[48,49] Graphene oxide (GO) was prepared according to the Hummers method, and graphene sheets were produced by reducing GO in the presence of PSS.[39] In this study, PSS was synthesized in an aqueous phase using 2,2′-azobis(2-amidinopropane) dihydrochloride (AAPH) as a water-soluble initiator for free-radical polymerization.[50] During the reduction of GO, the PSS electrostatically covered both sides of the graphene sheets through electrostatic repulsion interactions between the anionic head groups ($-SO_3^-$) of PSS and the graphene; thus, the PSS-coated graphene sheets became directly dispersible in the aqueous phase. The PSS-coated graphene sheets (30 wt % with respect to DMSO-doped PEDOT:PSS) were inserted and dispersed in PEDOT:PSS solutions doped with 5 wt % DMSO via mechanical stirring and sonochemical treatment. The 30 wt % PSS aqueous solutions were introduced to the PEDOT:PSS/graphene solutions to obtain sufficient viscosity (more than $10^3$ cP) for screen-printing. Although increasing the amount of PSS reduces the conductivity of PEDOT:PSS, loading of PSS can minimize and sometimes prevent serious agglomeration of the graphene sheets due to the van der Waals forces between them.[39] This intensifies the $\pi-\pi$ interactions between the thiophene rings of PEDOT:PSS and the graphene sheets due to the improved compatibility.[22,38,42−45,51] Hydrous, amorphous $RuO_2$ NPs formed as a result of the reaction between $RuCl_3$ and NaOH, followed by low-temperature annealing (150 °C).[46,47] These hydrous $RuO_2$ NPs were anchored to the surface of PEDOT:PSS/graphene by chemical interactions between the residual oxygen-containing functional groups on graphene sheets and the $RuO_2$ NPs, or through the electrostatic interaction between the $Ru^{4+}$ cations of $RuO_2$ and the $SO_3^-$ anions of the PSS molecules.[29,30,46] Thus, the PSS molecules acted as electrostatic stabilizers that reduced the particle aggregation of $RuO_2$ NPs and facilitated redox reactions between $RuO_2$ NPs and the PEDOT:PSS/graphene surfaces. The ternary $RuO_2$/PEDOT:PSS/graphene, having an optimized solution viscosity, was formed as patterned on flexible plastic substrates using the screen-printing method; the patterned films have a uniform thickness of ca. 5 $\mu$m. Accordingly, the synergetic effects from PEDOT:PSS, graphene sheets, and $RuO_2$ NPs resulted in a higher specific capacitance for the system. The patterns obtained, which consisted of three components (PEDOT:PSS, graphene, and $RuO_2$), were used as the working electrode of an electrochemical capacitor. The prepared $RuO_2$/PEDOT:PSS/graphene solutions showed good adhesion with the flexible PET, which was attributed to the optimized solution viscosity caused by PSS binders within the conducting inks. It was evident that the screen-printing method could be a facile means for forming thin-film electrodes of different shapes, sizes, and thicknesses on flexible plastic substrates.

Figure 1 shows field-emission scanning electron microscopy (FE-SEM) images of PEDOT:PSS, graphene, PEDOT-G30 (PEDOT:PSS with 30 wt % graphene), and $RuO_2$/PEDOT-G30 prepared by screen-printing. PEDOT:PSS was composed of nanoscale grains (diameter ca. 20−30 nm) (Figure 1a,b). The sizes of the graphene sheets ranged from ∼2 to 10 $\mu$m (Figure 1c,d and Supporting Information, Figure S1a); these graphene sheets were mixed with the PEDOT:PSS grains and became highly dispersed throughout the PEDOT:PSS surface, demonstrating that the graphene sheets could be successfully incorporated into the PEDOT:PSS system in the presence of amphiphilic PSS molecules (Figure 1e,f). An increased number of anionic groups per unit chain length of PSS molecules should enhance the interfacial interactions and mechanical


DOI: 10.1021/acsami.5b00657
ACS Appl. Mater. Interfaces 2015, 7, 10213−10227

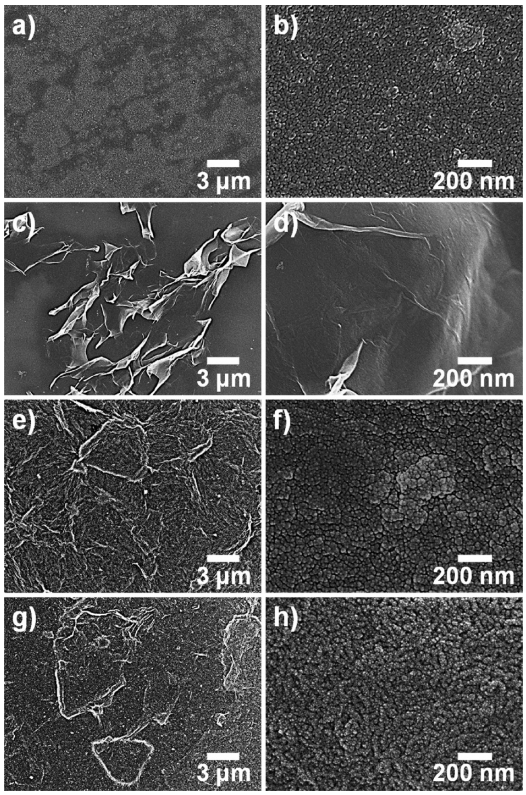


**Figure 1.** FE-SEM images of PEDOT:PSS (a, b), graphene (c, d), PEDOT-G30 (e, f), and $RuO_2$/PEDOT-G30 (g, h). Magnifications: 5000× (a, c, e, g) and 80000× (b, d, f, h).

interlocking between the graphene sheets and PEDOT:PSS nanograins, which would eventually lead to good dispersion of hydrophobic graphene sheets in an aqueous PEDOT:PSS system.[9,22,38,39,51] This, in turn, may increase the $\pi-\pi$ interactions between the PEDOT:PSS and graphene sheets, which is an important factor for increasing the conductivity of the nanocomposite. The $RuO_2$ NPs (<5 nm in size) were highly dispersed over the PEDOT-G30 surface (Figure 1g,h), and the sizes of the NPs were identical to those of $RuO_2$ NPs (Supporting Information, Figure S1b).[46] These $RuO_2$ NPs may become thermodynamically stable through electrostatic interactions between the cations ($Ru^{4+}$) and anions ($SO_3^-$), preventing incomplete redox reactions of $RuO_2$ NPs.[29,30]

Atomic force microscopy (AFM) was used to further investigate the morphological features of PEDOT−PSS nanocomposites affected by the $RuO_2$ NPs and graphene sheets (Figure 2). Compared with PEDOT:PSS (3.75 nm), the PEDOT-G30 (5.05 nm) exhibited rough surfaces due to the presence of graphene sheets (<5 nm thick sheets) (Figure 2a−c). Only a slight increase in the surface roughness should not have a significant effect on the charge carrier mobility within the nanostructures. However, the $\pi-\pi$ stacking between the PEDOT:PSS and graphene sheets resulted in a higher charge-carrier mobility within the nanocomposites.[22,38,42−45,51] Upon exposure to the electrolyte, this very small change in surface roughness can increase the contact surface area available for transporting electrons.[28] The increase in surface roughness (5.75 nm) induced by the $RuO_2$ NPs was relatively small, while the $RuO_2$ NPs provided faster, facile redox reactions of the PEDOT-G30 with the electrolyte (Figure 2d). Thus, it is reasonable to assume that the graphene sheets and $RuO_2$ NPs induced optimized morphologies to achieve better charge transport within the nanocomposites.

Raman spectroscopy was used to confirm the chemical bonding between PEDOT:PSS, graphene, and $RuO_2$ NPs (Figure 3a). The spectrum of graphene indicated two distinctive peaks: D mode (corresponding to structural defects (1351 $cm^{-1}$)) and G mode (related to the vibration of $sp^2$-hybridized carbon (1598 $cm^{-1}$)).[22,38,42−44,46] The D/G ratio of graphene was higher than that for nonreduced GO, suggesting that the defects in the graphene sheets were caused by GO reduction. In the spectrum of PEDOT:PSS, the major peaks for PEDOT indicated $SO_2$ bending (436 $cm^{-1}$), symmetric C−S−C deformation (701 $cm^{-1}$), oxyethylene ring deformation (575 and 987 $cm^{-1}$), C−O−C deformation (1093 $cm^{-1}$), C−C inter-ring stretching (1258 $cm^{-1}$), single C−C stretching (1364 $cm^{-1}$), C═C symmetrical stretching (1441 $cm^{-1}$), C═C asymmetrical stretching (1510 $cm^{-1}$), and C═C antisymmetrical stretching (1567 $cm^{-1}$).[15,22,38,42−44] The peaks of PSS observed at 1001, 1133, and 1600 $cm^{-1}$ were assigned to the vibration modes of C−C aromatic stretching, $SO_2$, and aromatic C−CH quadrant stretching, respectively.[53] When the graphene sheets were added to the PEDOT:PSS, the peaks associated with C═C symmetric and C═C asymmetric stretching in PEDOT:PSS became dominant, and the peak associated with C═C symmetrical stretching shifted from 1441 to 1446 $cm^{-1}$. These results suggest that the expanded-coil conformation became dominant within the PEDOT-G30 structure through strong $\pi-\pi$ interactions between the PEDOT:PSS and graphene sheets.[22,42−44] The structural change of the PEDOT:PSS is expected to increase the $\pi$-conjugation lengths of delocalizing electrons along the PEDOT:PSS backbone. When the $RuO_2$ NPs were incorporated into the PEDOT-G30, weak peaks at 513, 625, and 692 $cm^{-1}$, ascribed to hydrous $RuO_2$ with an amorphous structure, were observed.[46] Judging from these results, the PEDOT:PSS, graphene sheets, and $RuO_2$ NPs coexisted and maintained their individual electronic properties within the $RuO_2$/PEDOT-G30 nanocomposite. Figure 3b shows X-ray diffraction (XRD) patterns of graphene, PEDOT:PSS, PEDOT-G30, and $RuO_2$/PEDOT-G30 nanocomposites. In the spectrum of graphene, a broad peak at $2\theta = 24.5°$ with an interlayer distance of 3.63 Å was observed, which is close to that of graphite (3.39 Å).[22,55] Two distinctive peaks were observed at $2\theta = 18.0°$ (4.93 Å) and 26.4° (3.38 Å) for PEDOT:PSS, which were identical to the distances associated with interchain packing of the pseudo-orthorhombic crystal structure and the face-to-face interchain stackings of thiophene rings, respectively.[22,54] After the addition of PSS-coated graphene sheets into PEDOT:PSS, the characteristic features of the graphene sheets became indistinguishable, implying that the PSS-coated graphene sheets were highly dispersible with the PEDOT:PSS.[22] After the addition of $RuO_2$ NPs into the PEDOT-G30 nanocomposite, no significant peaks for crystalline $RuO_2$ were found, as opposed to the prominent peaks that appeared in the spectrum of pure $RuO_2$ NPs in the previous literature.[46] Thus, these results revealed that the $RuO_2$ NPs decorating the PEDOT-G30 nanocomposite were hydrous and amorphous and are, thereby, known to have high electrical and electrochemical properties.[46]

X-ray photoelectron spectroscopy (XPS) was used to identify the binding energy that reflects the elemental information on the PEDOT:PSS-based nanocomposites. Figure 4a shows fully scanned XPS patterns of PSS-coated graphene, PEDOT:PSS, PEDOT-G30, $RuO_2$, and $RuO_2$/PEDOT-G30. The spectra of


DOI: 10.1021/acsami.5b00657
ACS Appl. Mater. Interfaces 2015, 7, 10213−10227

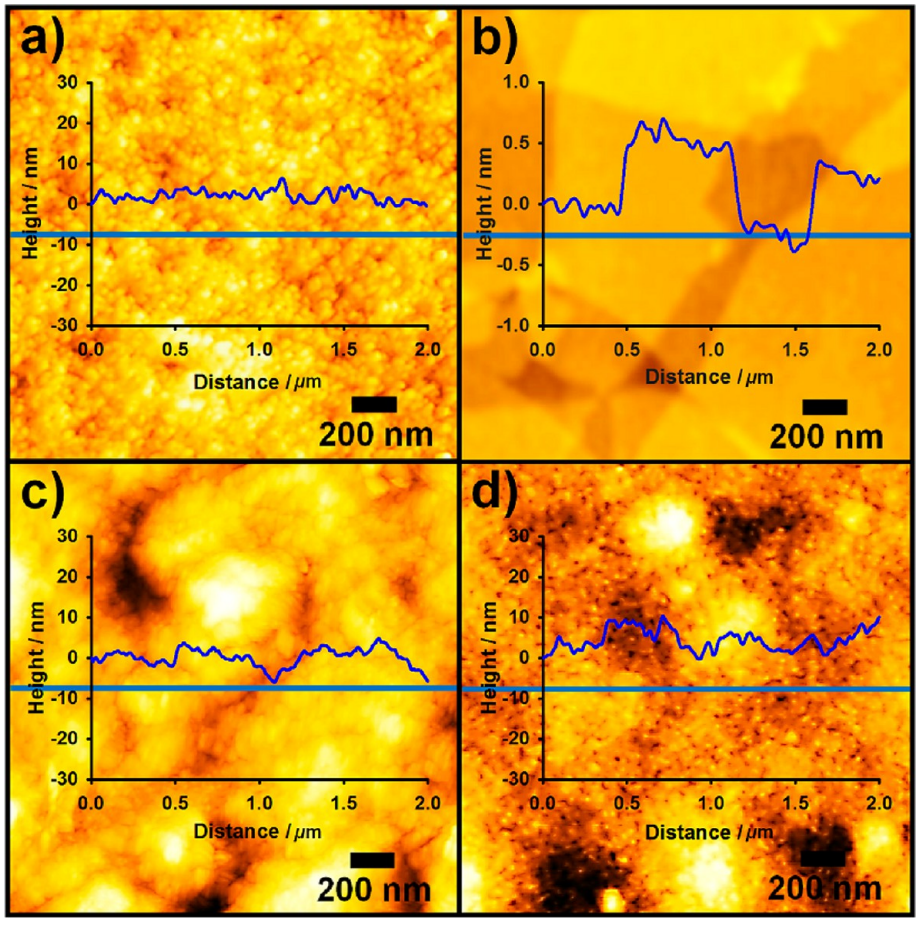


**Figure 2.** AFM images of (a) PEDOT:PSS, (b) graphene, (c) PEDOT-G30, and (d) $RuO_2$/PEDOT-G30.

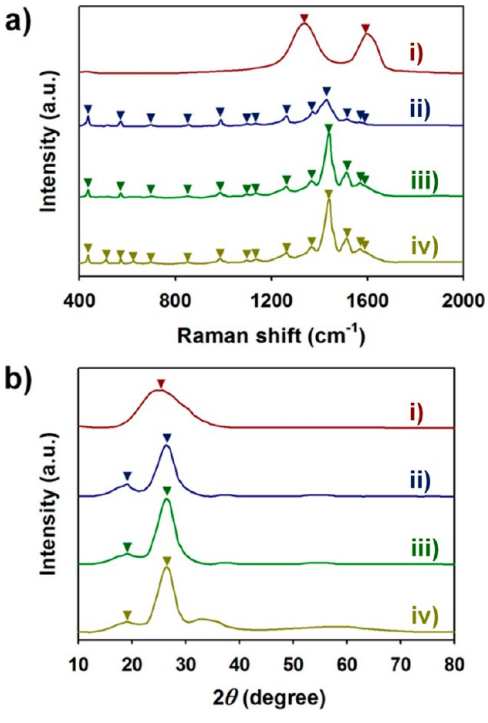


**Figure 3.** (a) Raman spectra and (b) XRD patterns of graphene (red), PEDOT:PSS (blue), PEDOT-G30 (green), and $RuO_2$/PEDOT-G30 (olive green).

the PEDOT:PSS-based nanocomposites exhibited four peaks located at 285, 533, 164, and 231 eV corresponding to C(1s), O(1s), S(2p), and S(2s), respectively.[54] In the XPS survey spectrum of PSS-coated graphene, weak peaks were observed at S(2p) (164 eV), S(2s) (231 eV), and N(1s) (400 eV). By comparing the XPS spectra and elemental compositions of PSS, graphene, and PSS-coated graphene, it was evident that the peaks for S(2p) and S(2s) were attributed to the PSS, and the N(1s) peak was observed in the spectrum of graphene (Supporting Information, Figure S2 and Table S1). Therefore, it can be considered that the graphene sheets have been successfully reduced with hydrazine in the presence of PSS molecules. The amounts of PSS attached on the graphene surfaces were estimated using XPS elemental composition (Supporting Information, Table S1). Considering that the graphene does not contain any sulfur, sulfur content in the PSS-coated graphene originates from the PSS.[39] Therefore, we could estimate the amount of PSS using eq 1:

$$\frac{S_{\text{PSS-coated graphene}}\ (\%)}{S_{\text{PSS}}\ (\%)} \cdot 100\% = \frac{5.70\%}{17.15\%} \cdot 100\% = 33.23\% \quad (1)$$

where $S_{\text{PSS-coated graphene}}$ and $S_{\text{PSS}}$ denote the sulfur contents of PSS-coated graphene and PSS, respectively. The result means that the 33.52% of sulfur is present on the graphene surface; thereby, it is assumed that 33.52% of PSS was combined with the graphene. In order to obtain more reliable results of the elemental composition of PSS-coated graphene, the elemental


DOI: 10.1021/acsami.5b00657
ACS Appl. Mater. Interfaces 2015, 7, 10213−10227

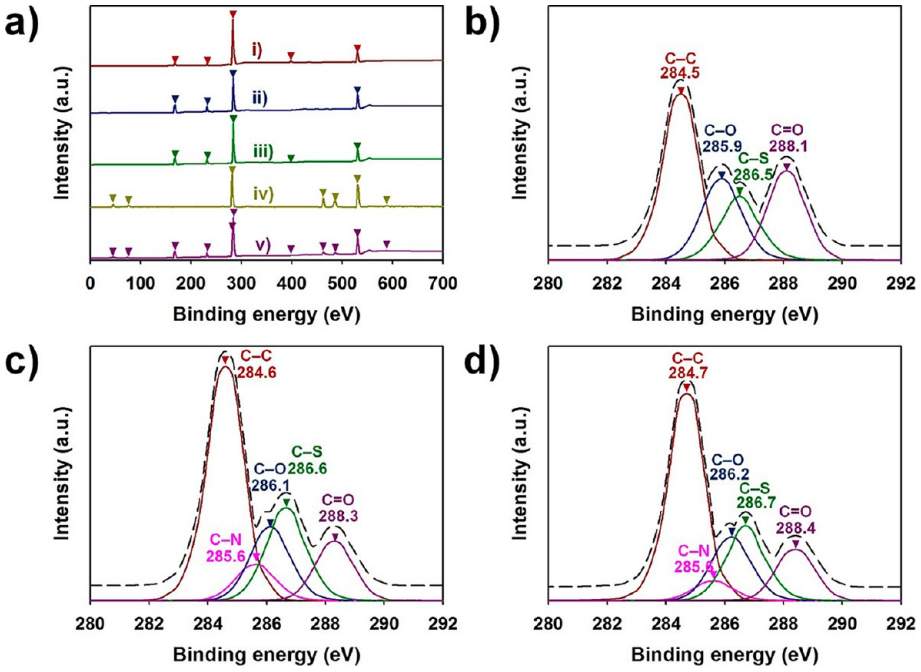


**Figure 4.** (a) Fully scanned XPS patterns of PSS-coated graphene (red), PEDOT:PSS (blue), PEDOT-G30 (green), $RuO_2$ (olive green), and $RuO_2$/PEDOT-G30 (purple). (b–d) C(1s) core spectra of (b) PEDOT:PSS, (c) PEDOT-G30, and (d) $RuO_2$/PEDOT-G30.

analysis of graphene, PSS, and PSS-coated graphene was further carried out using a combustion elemental analyzer (Supporting Information, Table S2). When the sulfur contents of PSS (18.41%) and PSS-coated graphene (6.39%) obtained using the combustion elemental analyzer were inserted into eq 1, the amount of PSS present on the graphene surface was estimated to be 34.7%. This result implies that the elemental composition obtained using the combustion elemental analyzer is in close accordance with the XPS results. The C content in the PEDOT:PSS/graphene became higher than in the PEDOT:PSS due to the presence of PSS-coated graphene.[38,54,76] The peaks at Ru(4p) (44.5 eV), Ru(4s) (75.0 eV), Ru(3d) (281.3 eV), Ru(3p) (463.0 and 485.0 eV), and Ru(3s) (588.0 eV) appeared in the XPS spectrum of $RuO_2$ NPs. According to a previous report, the binding energy of $Ru(3d_{5/2})$ occurs at 280.1 eV, while, upon oxidation of Ru, the peak shifts to higher binding energy (281.0 eV).[77] Thus, the binding energy of Ru(3d) (281.3 eV) corresponded to the binding energy of $Ru^{4+}$, suggesting the successful formation of hydrous $RuO_2$ NPs.[46,77] Furthermore, the peaks for the hydrous $RuO_2$ NPs were also found in the XPS spectrum of $RuO_2$/PEDOT-G30, implying the presence of $RuO_2$ in PEDOT-G30. In addition, the O content in the $RuO_2$/PEDOT-G30 nanocomposite became slightly higher than that of the PEDOT-G30 nanocomposite because of the presence of Ru–O in $RuO_2$. Figure 4b–d shows the C(1s) spectra of PEDOT:PSS, PEDOT-G30, and $RuO_2$/PEDOT-G30. When PSS-coated graphene was added to PEDOT:PSS, the intensities of C–C and C–S in the C(1s) spectrum were strengthened, which may be related to the presence of graphene and PSS. In addition, all peaks in the spectrum of PEDOT-G30 shifted slightly toward higher binding energy levels. According to the previous literature, these red shifts are related to the enhanced face-to-face interchain stacking of thiophene rings within the PEDOT:PSS structure through strong $\pi$–$\pi$ intermolecular interactions between the basal plane of the graphene sheets and the thiophene rings of the PEDOT:PSS structure.[22,38] The peak for C–N originated from the presence of hydrazine in the reduced graphene sheet. Moreover, further movement of C–C, C–O, C–S, and C=O peaks toward higher binding energy was observed when hydrous $RuO_2$ NPs were added to PEDOT-G30. This result implies that the carrier concentrations in the graphene sheets can be enhanced by additional electrons from PEDOT:PSS and hydrous $RuO_2$ NPs, resulting in a blue shift in the Fermi level.[22,38,46,77] These results, taken as a whole, suggest that the charge transport in the electrode material is enhanced by the synergetic effects from PEDOT:PSS, graphene sheets, and $RuO_2$ NPs.

**Application in Supercapacitor.** The electrode material is required to be highly conductive to enhance the charge collection capability of the capacitor.[42–44] In order to understand the effects of DMSO on the conductivity of PEDOT:PSS, the conductivity of PEDOT:PSS doped with various loadings of DMSO (0–15 wt %) was investigated (Supporting Information, Figures S3 and S4). In general, the DMSO interacts with the PSS via hydrogen bonding interactions, consequently reducing the electrostatic interactions between the PEDOT and PSS (Supporting Information, Figure S3).[78] Therefore, the insulating layers of PSS surrounding conductive grains of PEDOT became thinner, and the average sizes of PEDOT became larger with increasing DMSO loading.[2–4,15,16,28,78,79] Meanwhile, the increased grain sizes of PEDOT mean a longer average distance between conductive grains; thus, the excess DMSO can reduce the conductivity of PEDOT:PSS.[79] Although the optimal amounts of DMSO for PEDOT:PSS have been reported differently from a variety of research groups, the optimization of DMSO loading has been an important factor for increasing the conductivity of PEDOT.[2–4,15,16,28,78,79] Under our experimental conditions, we observed that the conductivity of PEDOT:PSS reaches the maximum value (910 S $cm^{-1}$) at the DMSO loading of 5 wt %, which is almost identical with the conductivity reported by Heraeus (900 S $cm^{-1}$) (Supporting Information, Figure


DOI: 10.1021/acsami.5b00657
ACS Appl. Mater. Interfaces 2015, 7, 10213–10227

S4).[16−18] Therefore, 5 wt % was chosen as an optimal amount of DMSO to enhance the conductivity of PEDOT:PSS.

To identify the optimal amount of graphene sheets to enhance the electrical and electrochemical properties of PEDOT:PSS/graphene nanocomposites, various amounts of graphene sheets (0−40 wt % in comparison with the nanocomposites) were incorporated into PEDOT:PSS (Figure 5). Based on the data in the Supporting Information, Figure S5,

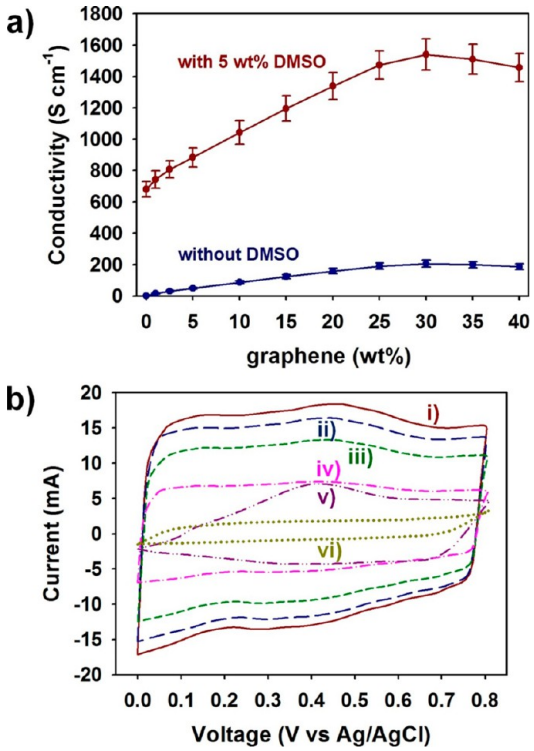


**Figure 5.** (a) Conductivity of PEDOT:PSS/graphene nanocomposites as a function of PSS-coated graphene content with 5 wt % DMSO and without DMSO. (b) Cyclic voltammograms of PEDOT-G30 (with 30 wt % graphene) (red), PEDOT-G40 (with 40 wt % graphene) (blue), PEDOT-G20 (with 20 wt % graphene) (green), PEDOT-G10 (with 10 wt % graphene) (pink), PEDOT:PSS (purple), and graphene (olive green) at a scan rate of 20 mV s$^{-1}$ in 0.5 M $H_2SO_4$.

the conductivity of the PEDOT:PSS/graphene nanocomposites was measured (Figure 5a).[52] The conductivity of PEDOT:PSS (680 S cm$^{-1}$) used in our work was lower than the conductivity measured in the Supporting Information, Figure S4, due to the presence of PSS binders that were added to PEDOT:PSS for the screen-printing process.[16−18] In comparison with PEDOT:PSS, the conductivity of PEDOT:PSS/graphene nanocomposites increased with the amount of graphene sheets, up to 30 wt %. Specifically, we observed that the conductivity of PEDOT-G30 increased 2-fold (1540 S cm$^{-1}$) compared with PEDOT:PSS. These results suggest that the appropriate amount of graphene sheets greatly enhanced the current collection of the PEDOT:PSS-based nanocomposites. This enhanced current collection may be attributed to strong $\pi-\pi$ stacking interactions between the aromatic structures of the PEDOT:PSS and graphene sheets, which may have elongated the conjugation lengths of transporting and hopping charge carriers within the PEDOT:PSS structure.[22,38,42−44,51] However, the conductivity of PEDOT:PSS/graphene became smaller after adding graphene sheets at contents that exceeded 30 wt %, implying that excessive amounts of graphene sheets may induce aggregation, which, in turn, would degrade the electrical performance of the electrode materials. Thus, this content was chosen to enhance the conductivity of the PEDOT:PSS nanostructure. Cyclic voltammetry (CV) studies were also carried out to determine the optimum additive graphene sheet content (Figure 5b and Supporting Information, Figure S6). The anodic peaks ranging from 0.40 to 0.50 V and the cathodic peaks ranging from 0.25 to 0.35 V in the CV curves of PEDOT:PSS/graphene nanocomposites were ascribed to oxidization and reduction reactions, respectively, given by

$$\mathrm{PEDOT^+{\cdot}PSS^- + e^- + H^+\ (oxidized\ state)} \leftrightarrows \mathrm{PEDOT^0{\cdot}PSS^-{\cdot}H^+\ (reduced\ state)} \quad (2)$$

where $e^-$ and $H^+$ denote the electron and proton in the $H_2SO_4$ electrolyte, respectively.[27] With increasing amounts of graphene sheets within the PEDOT:PSS, the pair of redox peaks became indistinguishable and the shape of the CV curves became more rectangular compared with PEDOT:PSS (Figure 5b). These rectangular-shaped CV curves may be associated with the electrochemical double-layer capacitance (EDLC) mechanism of the graphene sheets. Furthermore, it was obvious that PEDOT-G30, with 30 wt % graphene sheets, exhibited the largest CV area among the prepared samples at every scan rate, in accordance with the conductivity results (Supporting Information, Figure S6). This implies that a sufficient amount of $\pi$-electrons in the graphene sheets promotes $\pi-\pi$ stacking interactions with the thiophene rings of PEDOT:PSS, resulting in enhanced charge transfer in the PEDOT:PSS-based nanocomposites with the $H_2SO_4$ electrolyte.[22,38,42−45,51] The electrochemical activity between the electrode material and $H_2SO_4$ decreased when the added graphene sheet content exceeded 30 wt %, which may be related to the aggregation of excessive amounts of graphene sheets. Considering the conductivity and CV results, 30 wt % graphene sheets was selected as the optimal amount for the PEDOT:PSS-based nanocomposite.

To confirm the relationship between the morphological characteristics and conductivity of the samples, the surface resistance distribution for each 1 cm square pattern of the PEDOT:PSS, PEDOT-G30, and $RuO_2$/PEDOT-G30 electrodes was further analyzed (Figure 6). The screen-printing method provided good interplanar contact, and the surface resistances decreased after the addition of graphene sheets to the PEDOT:PSS structure (Figure 6a,b). These results imply that the restored graphitic network of $sp^2$ bonds played an important role in enhancing the $\pi$-interactions between the graphene sheets and PEDOT nanostructure, which eventually extended the conjugation length of the PEDOT chain.[22,38,41−45,51] Hence, PEDOT-G30 and $RuO_2$/PEDOT-G30 nanocomposites could conduct more current at the working electrode of the electrochemical capacitor, which is an important factor for obtaining high specific capacitances. After the addition of infinitesimal amounts of $RuO_2$ NPs, a slight decrease in the surface resistance was observed (Figure 6c). Based on the data, the conductivity of $RuO_2$/PEDOT-G30 was 1570 S cm$^{-1}$, which was slightly larger than that of PEDOT-G30 (1540 S cm$^{-1}$). This may suggest that the hydrous $RuO_2$ NPs used in our method have metallic conductivity, as reported by a previous paper in the literature ($10^{-3}$ Ω cm).[80]


DOI: 10.1021/acsami.5b00657
ACS Appl. Mater. Interfaces 2015, 7, 10213−10227

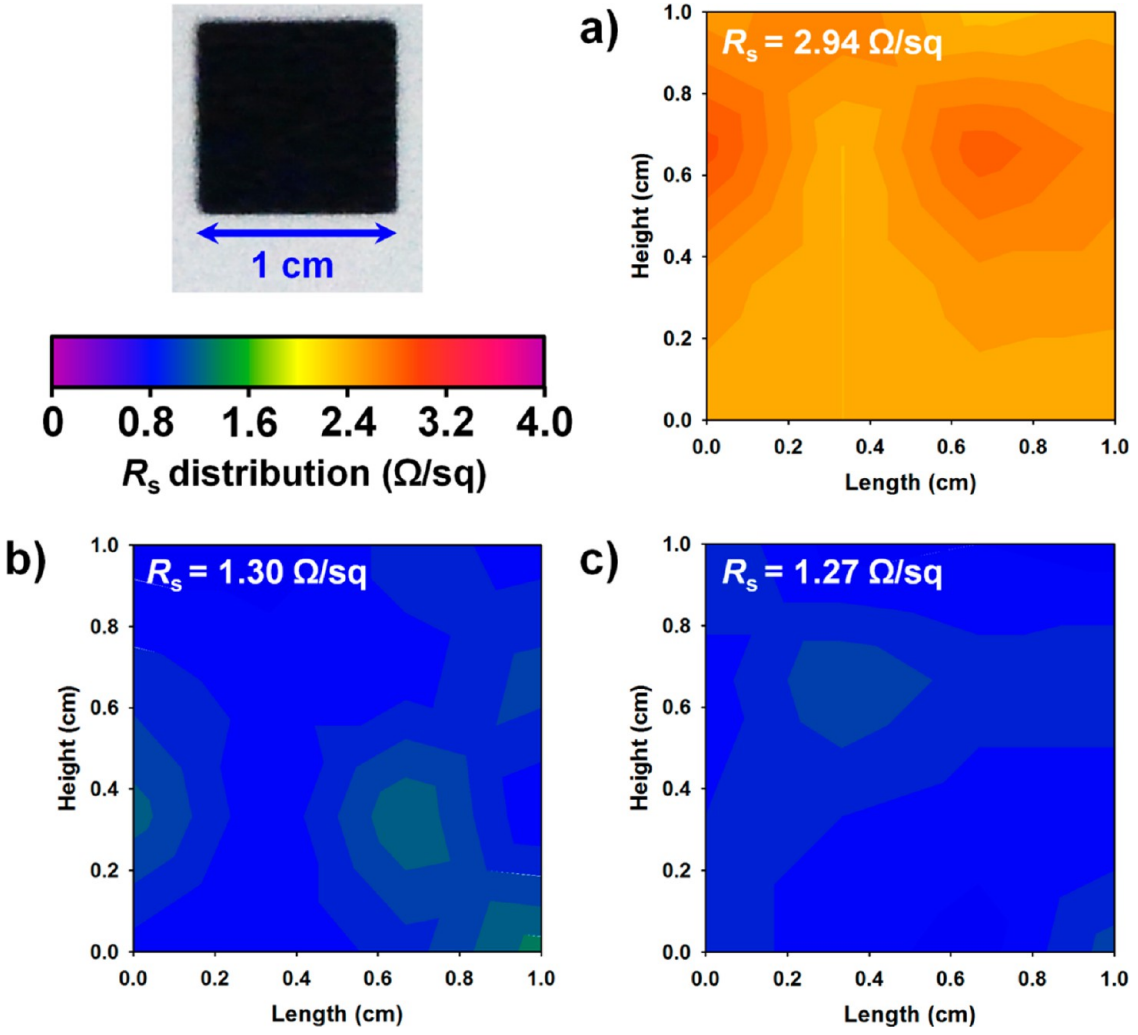


**Figure 6.** Distribution of surface resistances of (a) PEDOT:PSS, (b) PEDOT-G30, and (c) $RuO_2$/PEDOT-G30.

The CVs of PEDOT:PSS, graphene, $RuO_2$, $RuO_2$-G50 ($RuO_2$ with 50 wt % graphene), PEDOT:PSS/PEDOT-G30, and $RuO_2$/PEDOT-G30 were measured in a 0.5 M $H_2SO_4$ electrolyte at scan rates of 20 mV $s^{-1}$ (Figure 7a). In comparison with the CV curve of the PEDOT:PSS/graphene nanocomposite, a pair of very pronounced and reversible redox peaks are observed for $RuO_2$, $RuO_2$-G50, and $RuO_2$/PEDOT-G30 nanocomposite at every scan rate (Supporting Information, Figure S7). In the CV curve of $RuO_2$, the anodic peaks ranging from 0.40 to 0.75 V and the cathodic peaks ranging from 0.26 to 0.62 V were ascribed to oxidization and reduction reactions, respectively, given by

$$RuO_2 + 2e^- + 2H^+ \text{ (oxidized state)} \leftrightarrows Ru(OH)_2 \text{ (reduced state)} \quad (3)$$

where $e^-$ and $H^+$ indicate the electron and proton in the $H_2SO_4$ electrolyte, respectively.[72,73] The CV area became larger in the following order: graphene < PEDOT:PSS < PEDOT-G30 < $RuO_2$-G50 < $RuO_2$/PEDOT-G30 < $RuO_2$. These results indicate that hydrous $RuO_2$ NPs are redox-active, capable of faradaic energy storage via their pseudocapacitive behavior.[46] Thus, the $RuO_2$ NPs enabled faster oxidation/reduction reactions and charge transport into/out of the electrode, resulting in enhanced charge−discharge performance and larger specific capacitances of the samples. Hence, the synergetic effects from PEDOT:PSS, graphene sheets, and $RuO_2$ NPs delivered the expected enhancement in electrochemical performance. Figure 7b shows the galvanostatic charge−discharge curves of $RuO_2$, $RuO_2$/PEDOT-G30, $RuO_2$-G50, PEDOT-G30, and PEDOT:PSS at a current density of 0.5 A $g^{-1}$ over the voltage range of 0−0.8 V. The linear voltage−time profile and the highly symmetric charge−discharge characteristics imply facile redox reactions and charge transport into/out of the PEDOT:PSS-based nanocomposites during the charge/discharge process. The discharge time of the nanocomposites (given in seconds (s)) increased in the following order: graphene (542) < PEDOT:PSS (936) < PEDOT-G30 (2525) < $RuO_2$-G50 (3490) < $RuO_2$/PEDOT-G30 (3936) < $RuO_2$ (4641); these discharge times were proportional to the specific capacitances of the PEDOT:PSS-based nanocomposites. The specific capacitances were 967, 820, 727, 526, 195, and 113 F $g^{-1}$ for $RuO_2$, $RuO_2$/PEDOT-G30, $RuO_2$-G50, PEDOT-G30, PEDOT:PSS, and graphene nanocomposites respectively, at a current density of 0.5 A $g^{-1}$ (Figure 7c). The discharge time and specific capacitances of graphene, PEDOT-G30, $RuO_2$-G50, and $RuO_2$/PEDOT-G30 gradually decreased with increasing current density, whereas PEDOT:PSS and $RuO_2$ exhibited a rapid decrease in its specific capacitance when higher currents were applied (Figure 7c and Supporting


DOI: 10.1021/acsami.5b00657
ACS Appl. Mater. Interfaces 2015, 7, 10213−10227

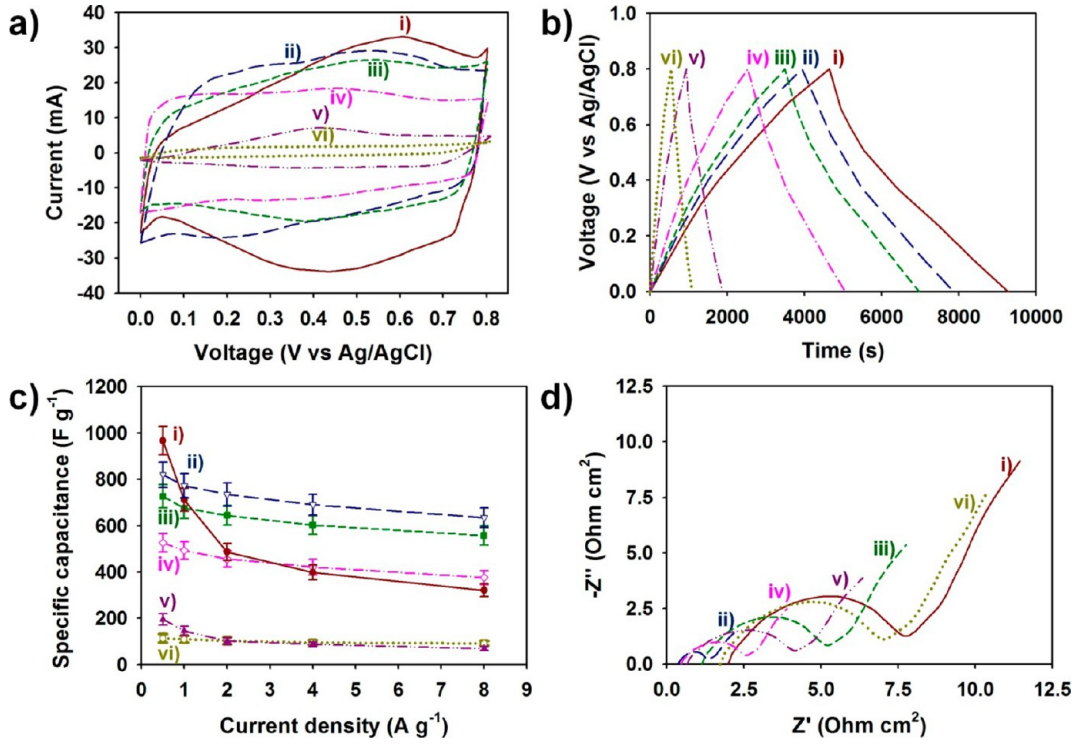


**Figure 7.** (a) Cyclic voltammograms at 20 mV $s^{-1}$ in 0.5 M $H_2SO_4$ electrolyte. (b) Galvanostatic charge−discharge characteristics at a current density of 0.5 A $g^{-1}$. (c) Specific capacitances (SCs) at different current densities (0.5−8.0 A $g^{-1}$). (d) Electrochemical impedance spectra (EIS) in the frequency range from 100 kHz to 10 mHz of $RuO_2$ (red), $RuO_2$/PEDOT-G30 (blue), $RuO_2$-G50 (green), PEDOT-G30 (pink), PEDOT:PSS (purple), and graphene (olive green).

Information, Figure S8). At the inner active sites of the electrodes, it became difficult to sustain the redox reactions completely at higher current densities, resulting in a reduction in the electrochemical performance of the electrodes.[29−35,42−44] In addition, pseudocapacitive materials, including PEDOT:PSS and $RuO_2$ NPs, usually provide slower ion diffusions than the graphene sheets do, which causes difficulty for the PEDOT NPs and $RuO_2$ NPs to continue appropriate redox reactions at higher current densities.[29,30,46,72−74] This implies that the graphene sheet incorporated electrodes have a better rate performance than PEDOT:PSS and $RuO_2$ due to the enhanced chemical and mechanical stability provided by the graphene sheets in maintaining the redox reactions at higher current densities.[55] Consequently, the synergistic effects from the $RuO_2$ NPs, PEDOT:PSS nanostructures, and graphene sheets led to higher specific capacitances, which were consistent with enhanced electrochemical performances. To further identify the beneficial effects of the graphene sheets and the $RuO_2$ NPs on the charge transport within the ternary electrode system, series ($R_s$) and charge transfer resistances ($R_{ct}$) were measured using electrochemical impedance spectroscopy (EIS) (Figure 7d). The Nyquist impedance plots consisted of semicircular curves for high frequencies and linear curves for low frequencies.[27] In particular, the DMSO-induced PEDOT:PSS exhibited lower $R_s$ and $R_{ct}$ than the graphene sheets and $RuO_2$ NPs did. This indicates that the phase separation and uniform distribution of PEDOT and PSS in the PEDOT:PSS could be successfully achieved through the addition of DMSO, resulting in better charge transfer of the PEDOT:PSS.[2,28] As mentioned above, the low-rate capability of the $RuO_2$ NPs in Figure 7c is also ascribed to its high $R_{ct}$. Importantly, binary or ternary electrode systems, such as $RuO_2$/PEDOT-G30, PEDOT-G30, and $RuO_2$-G50, were more effective for lowering $R_s$ and $R_{ct}$ compared with one-component electrodes, including $RuO_2$, graphene, and PEDOT:PSS. The size of the semicircle and $R_{ct}$ significantly decreased after the addition of the graphene sheets and $RuO_2$ NPs, which was consistent with the CV test results. Moreover, the EIS results indicated that the ideal combination of PEDOT:PSS, $RuO_2$ NPs, and graphene sheets improved the interfacial charge transfer within the nanocomposite, which could lead to a better capacitive performance for electrochemical capacitors.

To examine the practical applicability of the $RuO_2$/PEDOT-G30 nanocomposites, Ragone plots of different electrode systems are shown in Figure 8. The energy density (Wh $kg^{-1}$) of samples at the power density of 67 W $kg^{-1}$ increased in the

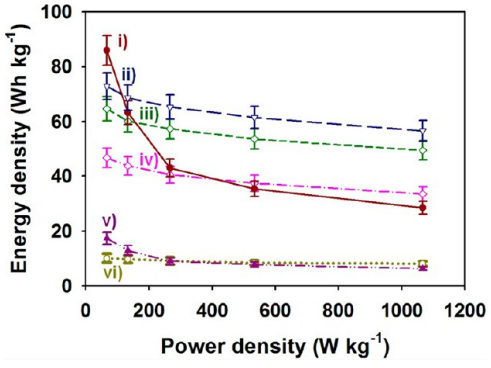


**Figure 8.** Ragone plot of electrochemical cells containing different electrodes: $RuO_2$ (red), $RuO_2$/PEDOT-G30 (blue), $RuO_2$-G50 (green), PEDOT-G30 (pink), PEDOT:PSS (purple), and graphene (olive green).


DOI: 10.1021/acsami.5b00657
ACS Appl. Mater. Interfaces 2015, 7, 10213−10227

following order: graphene (10) < PEDOT:PSS (17) < PEDOT-G30 (47) < $RuO_2$-G50 (65) < $RuO_2$/PEDOT-G30 (73) < $RuO_2$ (86). Although the highest energy density was achieved by using $RuO_2$ NPs (86 Wh $kg^{-1}$ at 67 W $kg^{-1}$), the energy density of $RuO_2$ rapidly decreased with increasing power density. On the other hand, the energy density of the $RuO_2$/PEDOT-G30 was highly preserved at higher power densities, and its energy density was the highest among the samples at power densities of 133, 266, 533, and 1067 W $kg^{-1}$. These results suggest that the $RuO_2$/PEDOT-G30 benefits from the advantages of each component: (1) $RuO_2$ can store more energy than the graphene and PEDOT:PSS because of its excellent redox behaviors. (2) PEDOT:PSS prevented $RuO_2$ NPs from aggregating and detaching from the substrate through the electrostatic interactions between PSS and $Ru^{4+}$ cations. (3) The graphene provides rapid sorption and desorption of ions at the electrode surfaces.[29,30,39,42−44,46,72−76]

The cycling stabilities of the electrochemical capacitors based on the $RuO_2$/PEDOT-G30, PEDOT-G30, and PEDOT:PSS were measured with galvanostatic charge−discharge cycles at a current density of 0.5 A $g^{-1}$ (Figure 9). After 1000 such cycles,

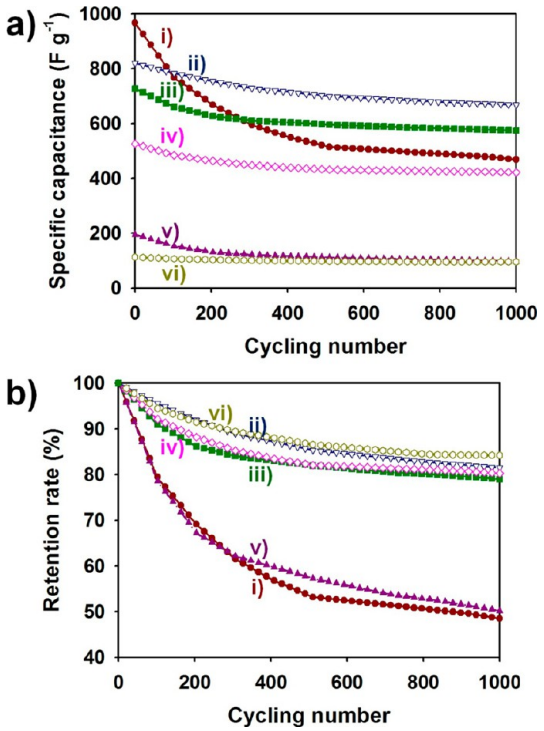


**Figure 9.** Long-term cycling stability of electrochemical capacitors containing $RuO_2$, $RuO_2$/PEDOT-G30, $RuO_2$-G50, PEDOT-G30, PEDOT:PSS, and graphene: (a) specific capacitance and (b) retention rate upon completion of 1000 cycles.

the specific capacitances of the $RuO_2$/PEDOT-G30, $RuO_2$-G50, $RuO_2$, PEDOT-G30, graphene, and PEDOT:PSS nanocomposites decreased to 668, 574, 469, 422, 98, and 95 F $g^{-1}$, respectively, from their initial specific capacitances (Figure 9a). The retention rate of the nanocomposites (given in %) increased in the following order: $RuO_2$ (48.5) < PEDOT:PSS (50.2) < $RuO_2$-G50 (79.0) < PEDOT-G30 (80.3) < $RuO_2$/PEDOT-G30 (81.5) < graphene (84.2) (Figure 9b). Despite their high capacitance and energy density, the $RuO_2$ NPs exhibited the lowest retention rate among the samples due to their breaking and detaching from the PET substrate.[29,30,42−44,73] Furthermore, PEDOT usually suffers from degradation and shrinkage upon exposure to electrolyte during the repeated cycles.[29,30,73] These results indicated that the graphene sheets with high chemical and mechanical stabilities, and high flexibility, prevented the PEDOT:PSS and $RuO_2$ nanostructures from breaking, shrinking, and collapsing upon repeated cycling.[42−44,46,74] Additionally, it can be assumed that the improved dispersion of the graphene sheets and hydrous $RuO_2$ NPs through the electrostatic interactions with anions of the PSS resulted in better cycling performance of the $RuO_2$/PEDOT-G30 nanocomposite.[29,30,39]

Overall performances of state-of-art electrodes and our work are summarized in radar plots (Figure 10).[56] Our work has shown higher capacitance, energy density, and electrical conductivity than the other conducting polymer-based supercapacitors.[42,46,74,75] In particular, the capacitance of $RuO_2$/PEDOT-G30 (820 F $g^{-1}$) was more than 4 times higher than that of the $SnO_2$/graphene/PEDOT ternary electrode (184 F $g^{-1}$). Compared with previous work, the improved electrochemical performances of this work can be attributed to two advantages: (1) The PSS played an important role to promote the effective utilizations of three different components, including PEDOT:PSS, $RuO_2$, and graphene, by allowing electrostatic stabilization interactions with each component.[29,30,39] (2) Morphological homogeneity of electrode materials could be achieved by a screen-printing method, which allows high connectivity between PEDOT:PSS chains and uniform distribution of each component, including PEDOT:PSS, graphene, and $RuO_2$, in the nanocomposites.[9,36,37]

## CONCLUSIONS

The present work describes an efficient way to obtain highly defined electrode patterns for use as high-performance electrochemical capacitors by magnifying the synergetic effects from PEDOT:PSS, graphene, and $RuO_2$ NPs in an aqueous phase. The graphene sheets (size 2−10 $\mu$m) were readily reduced in the presence of high-molecular-weight PSS, and greatly enhanced the charge-transport properties of electrode materials through strong $\pi-\pi$ stacking interactions with the PEDOT:PSS structure. The $RuO_2$ NPs (diameter ~5 nm) were also highly dispersible in the PEDOT:PSS/graphene system, and acted as efficient catalysts to facilitate redox reactions with the protons ($H^+$) of the $H_2SO_4$ electrolyte. Experimental data obtained from various characterizations, such as the four-probe method, Raman spectroscopy, and the XRD, XPS, CV, and EIS techniques, demonstrated that the charge transport and electrochemical properties had significantly improved through the synergetic effects of the three components: PEDOT:PSS, graphene, and hydrous $RuO_2$. The solution-processed $RuO_2$/PEDOT:PSS/graphene electrode system exhibited a conductivity of 1570 S $cm^{-1}$, a specific capacitance of 820 F $g^{-1}$ at a current density of 0.5 A $g^{-1}$, and an energy density of 73 Wh $kg^{1-}$ at a power density of 67 W $kg^{-1}$. Moreover, the $RuO_2$/PEDOT:PSS/graphene-based capacitor showed improved cycling (81.5% after 1000 cycles) and rate performance. Such improvements were highly correlated with the synergetic effects of the PEDOT:PSS, graphene, and hydrous $RuO_2$ NPs. The procedure described herein can be used as an efficient means to produce highly conductive, electrochemically active electrode patterns for use as electrode materials in various energetic and environmental applications, such as solar cells, batteries, chemical sensors, and thin-film transistors.


DOI: 10.1021/acsami.5b00657
ACS Appl. Mater. Interfaces 2015, 7, 10213−10227

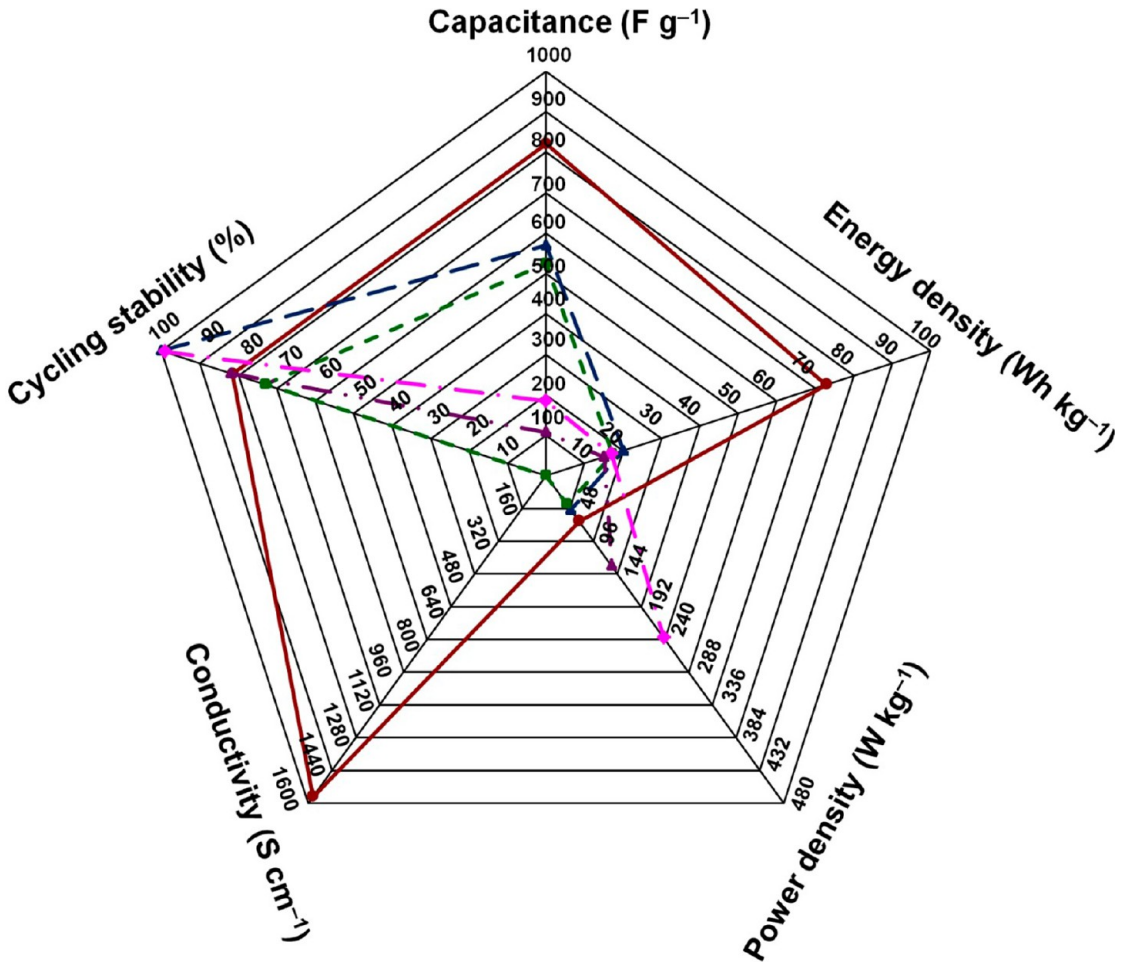


**Figure 10.** Radar plot to compare the present work with four supercapacitors cited from refs 42, 46, 74, and 75. Red, blue, green, pink, and purple curves are generated by connecting data points from supercapacitors using $RuO_2$/PEDOT-G30 (this work), $RuO_2$/graphene, PANI/carbon hollow nanoparticle, graphene/$SnO_2$/PEDOT, and RGO−PEDOT, respectively.

## EXPERIMENTAL SECTION

**Materials.** PEDOT:PSS solution (Clevios PH1000) was obtained from Heraeus Precious Metals GmbH & Co. (Leverkusen, Germany). The solid content and PEDOT to PSS ratio of the PH 1000 solution was 1−1.3% and 1:2.5 by weight, respectively. 4-Styrenesulfonic acid (4-SS), 2,2′-azobis(2-amidinopropane) dihydrochloride (AAPH), natural flake graphite, sodium nitrate ($NaNO_3$, 99%), hydrazine monohydrate ($N_2H_4{\cdot}H_2O$, 98%), and ruthenium(III) chloride hydrate ($RuCl_3{\cdot}nH_2O$, reagent plus) were obtained from Sigma-Aldrich (St. Louis, MO, USA). Potassium permanganate ($KMnO_4$, 99.3%) and phosphorus pentoxide ($P_2O_5$, extra pure) were purchased from Junsei Chemical Co. (Tokyo, Japan). Potassium persulfate ($K_2S_2O_8$, 99%) was purchased from Kanto Chemical Co. (Tokyo, Japan). Dimethyl sulfoxide (DMSO, 98%), sulfuric acid ($H_2SO_4$, 95%), sodium hydroxide (NaOH, 99%), sodium chloride (NaCl, 99%), hydrogen peroxide ($H_2O_2$, 30−35.5%), and hydrochloric acid (HCl, 35−37%) were purchased from Samchun (Seoul, Korea).

**Synthesis of PSS Solution.** 4-Styrenesulfonic acid (4-styrenesulfonic acid:distilled water = 30:70 by weight) was added into distilled water with vigorous stirring at 45 °C for 1 h. Polymerization of 4-styrenesulfonic acid was conducted by adding AAPH (0.03 mg $mL^{-1}$ in distilled water) at 45 °C for 12 h in a $N_2$ atmosphere. Weight-average molecular weight ($M_w$) of PSS was calculated using the GPC method, and the $M_w$ of PSS was as high as $1.96 \times 10^6$ Da.

**Synthesis of Hydrous $RuO_2$ NPs.** Hydrous $RuO_2$ NPs were synthesized according to the sol−gel method given as $RuCl_3$ + 3NaOH → $3Ru(OH)_3$ + 3NaCl.[46,47] To balance the pH to 7, 1 M NaOH solution was added into 100 mL of 0.1 M $RuCl_3$ with vigorous stirring for 1 h at 25 °C. The mixed solution was continuously stirred for 12 h, and then washed and centrifuged with distilled water several times to remove residual NaCl salts. The washed sample was dried at 150 °C for 12 h. The dried $RuO_2$ NPs were redispersed in distilled water by using an ultrasonicator (VCX 500, Sonics & Materials. Inc. USA) for 3 h in an ice bath. In the sample, the density of $RuO_2$ NPs in the distilled water was about 5 mg $mL^{-1}$. For further evaluation of the $RuO_2$-based electrode systems without PEDOT:PSS, two different electrode systems, including $RuO_2$ and $RuO_2$/graphene, have been prepared. To fabricate $RuO_2$ electrode for screen-printing, the $RuO_2$ solution ($RuO_2$ solution:PSS solution = 50:50 by weight) was poured into PSS solution and vigorously stirred for 2 h. As-prepared solution was sonochemically treated for 1 h to improve the dispersion of $RuO_2$ NPs in the PSS solution. $RuO_2$/graphene solution for screen-printing was prepared by adding PSS-coated graphene (PSS-coated graphene:$RuO_2$ solution = 50:50 by weight) into the $RuO_2$ solution with vigorous stirring and sonochemical treatment. As-prepared $RuO_2$ and $RuO_2$/graphene solutions were deposited onto the PET substrates via the screen-printing method.

**Synthesis of PSS-Coated Graphene.** Water-dispersible graphene sheets were prepared by using modified Hummers and Ruoff methods in the presence of synthesized PSS.[39] Preoxidation of natural graphite powders was carried out by dissolving 5 g of natural graphite powder, 2.5 g of $P_2O_5$, and 2.5 g of $K_2S_2O_8$ in 30 mL of $H_2SO_4$, and the mixed solution was heated at 80 °C for 6 h. The solution was filtered and washed using a cellulose acetate filter (Whatmann Inc., USA) with excess distilled water. The remaining powder was dried in a vacuum oven at 25 °C for 24 h. A 2.5 g sample of $NaNO_3$ was dissolved in 120 mL of $H_2SO_4$ solution, followed by addition of preoxidized graphite,


DOI: 10.1021/acsami.5b00657
ACS Appl. Mater. Interfaces 2015, 7, 10213−10227

and the solution was vigorously stirred for 0.5 h in an ice bath. A 15.0 g sample of $KMnO_4$ was slowly introduced into the solution within 45 min at a temperature lower than 20 °C, and the solution was heated at 35 °C for 4 h to obtain a brownish gray paste. In the next step, 600 mL of distilled water was slowly poured into into the solution, followed by the addition of 25 mL of $H_2O_2$ solution, and the color of the paste turned a bright yellow. The bright yellow solution was washed with 5 wt % HCl and distilled water several times to balance the pH of solution to 7, followed by sonochemical treatment to exfoliate graphitic oxide into graphene oxide. Then the solution was centrifuged at 6000 rpm for 40 min to exclude residue. As-prepared graphene oxide (GO) solution was dried in a vacuum oven at 40 °C for 24 h. The dried GO was poured into the diluted PSS solution (1 mg $mL^{-1}$ in distilled water, 3/1 w/w vs GO) with vigorous stirring, and the density of GO in the resulting solution was about 0.3 mg $mL^{-1}$. After dispersion of the GO powders into the PSS solution, hydrazine monohydrate (1/1000 v/v vs distilled water), a reducing agent, was added to the mixed solution with vigorous stirring at 95 °C for 1 h. After the reduction process in the presence of PSS, the PSS-coated reduced graphene oxide (RGO) solution was filtered using excess distilled water and dried in a vacuum oven at 25 °C for 24 h. As a result, water-dispersible and PSS-coated RGO powders were obtained.

**Synthesis of $RuO_2$/PEDOT:PSS/Graphene.** DMSO (DMSO:-PEDOT:PSS = 5:95 by weight) was added into PEDOT:PSS solution and followed by addition of the PSS-coated RGO (PSS-coated RGO:DMSO-PEDOT:PSS = 30:70 by weight) with vigorous stirring and sonochemical treatment. The synthesized PSS (30 wt % with respect to distilled water, 1/5 v/v vs PEDOT:PSS) was further introduced into the DMSO-PEDOT:PSS solution with vigorous stirring and sonochemical treatment. For comparison, screen-printable ink based on the PEDOT:PSS and graphene sheets were also prepared by the same procedure without the other components. In the next step, hydrous $RuO_2$ NPs (5 mg $mL^{-1}$ in distilled water, 1/10 w/w vs PEDOT:PSS/graphene) were added into the PEDOT:PSS/graphene solution with vigorous stirring and sonochemical treatment. $RuO_2$/PEDOT:PSS/graphene electrodes with a 1 cm square pattern were deposited on flexible poly(ethylene terephthalate) (PET) substrates by a screen-printing machine (SM-S320, Sun Mechanix Co., Seoul, Korea) using as-prepared $RuO_2$/PEDOT:PSS/graphene solutions. The electrode thicknesses were adjusted by the number of screen-printings, which also adjust the mass of screen-printed electrode. Ten times of screen-printing were conducted to form a pattern having a thickness of about 5.0 $\mu$m and an electrode mass of 3 mg. As-prepared screen-printed patterns were placed on the hot plate and dried at 100 °C on for 10 min.

**Electrochemical Measurements.** For the evaluation of electrochemical characteristics on the samples, cyclic voltammetry (CV) and galvanostatic charge/discharge measurements were observed in 1 M $H_2SO_4$ electrolyte solution using a WBCS 3000 potentiostat/galvanostat (Wonatech, Korea). Screen-printed electrodes, 1 cm square patterns deposited on PET substrates, served as working electrodes, and a platinum wire (CH Instruments, Inc., USA) was utilized as a counter electrode. Ag/AgCl in saturated KCl solution was used as a reference electrode. Cyclic voltammograms (CVs) of screen-printed electrodes were measured from 0 and 0.8 V at various scan rates (10, 20, and 50 mV $s^{-1}$). Galvanostatic charge/discharge experiments were performed by cycling the potential from 0 to 0.8 V at various current densities (0.5−8.0 A $g^{-1}$). Mass specific capacitances ($C_m$'s) of electrochemical cells were calculated using the equation $C_m$ (F $g^{-1}$) = $I\Delta t/m\Delta V$, where $I$, $\Delta t$, $m$, and $\Delta V$ denote the constant discharge current, discharge time, mass of a thin film, and voltage drop upon discharge, respectively.[55] The energy density of each sample was calculated by using the equation $E$ (Wh $kg^{-1}$) = $C_m(\Delta V)^2/2$, where $C_m$ and $\Delta V$ denote the mass capacitance of each sample and voltage drop upon discharge, respectively.[48] The power density of each sample was estimated using the equation $P$ (W $kg^{-1}$) = $E/t$, where $E$ and $t$ denote the energy density and discharge time of each sample, respectively.[72] Electrochemical impedance spectra (EIS) of the electrochemical cells were acquired in the frequency range of 100 kHz to 0.01 Hz using a ZIVE SP2 impedance analyzer (WonATech, Korea).

**Instrumental Analyses.** Surface images of the screen-printed electrodes were acquired with a field-emission scanning electron microscope (FE-SEM, JSM-6701F, JEOL, Japan) and an atomic force microscope (AFM; Innova SPM, Vecco, USA). Microscopic images of the graphene sheets and $RuO_2$ NPs were obtained with a transmission electron microscope (TEM; LIBRA 120, Carl Zeiss, Germany). Elemental analysis of graphene, PSS, and PSS-coated graphene was done using an X-ray photoelectron spectrometer (XPS; AXIS-His, Kratos/Shimadzu, Kyoto, Japan) and combustion elemental analyzer (Flash 2000 Analyzer, Thermo Scientific Inc., USA). The conductivity of nanocomposites (defined as $\sigma$ (S $cm^{-1}$) = $1/\rho$ = (ln $2/\pi t$)$(1/R)$, where $\rho$ is the static resistivity, $R$ is the surface resistance, and $t$ is the thickness of the electrode material) was measured using a four-point probe system (Mode Systems Co., Korea) equipped with a current-source meter (Keithley 2400, Keithley Co., USA).[52] The surface resistance distribution for each 1 cm square sample pattern of the samples was investigated to obtain reliable conductivity values for the samples. It was notable that every sample exhibited a narrow surface resistance distribution. This indicated that the highly uniform thin films could be deposited onto flexible PET substrates using the screen-printing method, resulting in enhanced connectivity between the conductive areas within the PEDOT:PSS thin films. X-ray diffractograms (XRDs) were measured with a SmartLab X-ray diffractometer (Rigaku Co., Tokyo, Japan). Raman spectra were measured on T6 (Horiba-Jobin Yvon Co., Tokyo, Japan) spectrometer. The $M_w$ value of PSS was measured by using an EcoSEC gel permeation chromatography (GPC) system (HLC-8320; Tosoh Co., Tokyo, Japan) with commercially available narrow molecular weight PSS samples as standards.

## ■ ASSOCIATED CONTENT

### Ⓢ Supporting Information

TEM images of graphene and $RuO_2$ nanoparticles; fully scanned XPS patterns of PSS, graphene, and PSS-coated graphene; XPS elemental composition of graphene, PSS, PSS-coated graphene, PEDOT:PSS, PEDOT-G30, $RuO_2$, and $RuO_2$/PEDOT-G30; elemental analysis of graphene, PSS, and PSS-coated graphene obtained using a combustion elemental analyzer; possible mechanism of interaction between PEDOT:PSS and DMSO; conductivity of PEDOT:PSS as a function of DMSO content (0−15 wt %); distribution of surface resistances of PEDOT:PSS, PEDOT-G10, PEDOT-G20, PEDOT-G30, and PEDOT-G40; cyclic voltammograms of graphene, PEDOT:PSS, PEDOT-G10, PEDOT-G20, PEDOT-G30, PEDOT-G40, $RuO_2$, $RuO_2$-G50, and $RuO_2$/PEDOT-30 at different scan rates (10−50 mV $s^{-1}$) in 0.5 M $H_2SO_4$; and galvanostatic charge−discharge characteristics of PEDOT:PSS, graphene, $RuO_2$, PEDOT-G30, $RuO_2$-G50, and $RuO_2$/PEDOT-G30 at different current densities (0.5−8.0 A $g^{-1}$). The Supporting Information is available free of charge on the ACS Publications website at DOI: 10.1021/acsami.5b00657.

## ■ AUTHOR INFORMATION

### Corresponding Author

*E-mail: jsjang@plaza.snu.ac.kr.

### Notes

The authors declare no competing financial interest.

## ■ ACKNOWLEDGMENTS

This work was supported by the Global Frontier R&D Program on Center for Multiscale Energy System funded by the National



DOI: 10.1021/acsami.5b00657
ACS Appl. Mater. Interfaces 2015, 7, 10213−10227

Research Foundation under the Ministry of Education, Science and Technology, Korea (2011-0031573).

## REFERENCES


(1) Groenendaal, L. B.; Jonas, F.; Freitag, D.; Pielartzik, H.; Reynolds, J. R. Poly(3,4-ethylenedioxythiophene) and Its Derivatives: Past, Present, and Future. *Adv. Mater.* **2000**, *12*, 481−494.

(2) Kim, J. Y.; Jung, J. H.; Lee, D. E.; Joo, J. Enhancement of Electrical Conductivity of Poly(3,4-ethylenedioxythiophene)/Poly(4-styrenesulfonate) by a Change of Solvents. *Synth. Met.* **2002**, *126*, 311−316.

(3) Ouyang, J.; Chu, C.-W.; Chen, F.-C.; Xu, Q.; Yang, Y. High-Conductivity Poly(3,4-ethylenedioxythiophene):Poly(styrene sulfonate) Film and Its Application in Polymer Optoelectronic Devices. *Adv. Funct. Mater.* **2005**, *15*, 203−208.

(4) Xia, Y.; Ouyang, J. Significant Different Conductivities of the Two Grades of Poly(3,4-ethylenedioxythiophene):Poly(styrenesulfonate), Clevios P and Clevios PH1000, Arising from Different Molecular Weights. *ACS Appl. Mater. Interfaces* **2012**, *4*, 4131−4140.

(5) Ouyang, J. Solution-Processed PEDOT:PSS Films with Conductivities as Indium Tin Oxide through a Treatment with Mild and Weak Organic Acids. *ACS Appl. Mater. Interfaces* **2013**, *5*, 13082−13088.

(6) Jang, J. Conducting Polymer Nanomaterials and Their Applications. *Adv. Polym. Sci.* **2006**, *199*, 189−259.

(7) Neoh, K. G.; Lau, K. K. S.; Wong, V. V. T.; Kang, E. T.; Tan, K. L. Structure and Degradation Behavior of Polypyrrole Doped with Sulfonate Anions of Different Sizes Subjected to Undoping-Redoping Cycles. *Chem. Mater.* **1996**, *8*, 167−172.

(8) Jang, J.; Ha, J.; Cho, J. Fabrication of Water-Dispersible Polyaniline-Poly(4-styrenesulfonate) Nanoparticles for Inkjet-Printed Chemical-Sensor Applications. *Adv. Mater.* **2007**, *19*, 1772−1775.

(9) Shin, K.-Y.; Cho, S.; Jang, J. Graphene/Polyaniline/Poly(4-styrenesulfonate) Hybrid Film with Uniform Surface Resistance and Its Flexible Dipole Tag Antenna Application. *Small* **2013**, *9*, 3792−3798.

(10) Lefebvre, M. C.; Qi, Z.; Pickup, P. G. Electronically Conducting Proton Exchange Polymers as Catalyst Supports for Proton Exchange Membrane Fuel Cells. Electrocatalysis of Oxygen Reduction, Hydrogen Oxidation, and Methanol Oxidation. *J. Electrochem. Soc.* **1999**, *146*, 2054−2058.

(11) Sun, X.; Hagner, M. Novel Poly(acrylic acid)-Mediated Formation of Composited, Poly(3,4-ethylenedioxythiophene)-Based Conducting Polymer Nanowires. *Macromolecules* **2007**, *40*, 8537−8539.

(12) Kim, J. Y.; Kim, S. H.; Lee, H.-H.; Lee, K.; Ma, W.; Gong, X.; Heeger, A. J. New Architecture for High-Efficiency Polymer Photovoltaic Cells Using Solution-Based Titanium Oxide as an Optical Spacer. *Adv. Mater.* **2006**, *18*, 572−576.

(13) Yeo, J.-S.; Yun, J.-M.; Kang, M.; Khim, D.; Lee, S.-H.; Kim, S.-S.; Na, S.-I.; Kim, D.-Y. An Approach for an Advanced Anode Interfacial Layer with Electron-blocking Ability to Achieve High-Efficiency Organic Photovoltaics. *ACS Appl. Mater. Interfaces* **2014**, *6*, 19613−19620.

(14) Wang, K.; Yi, C.; Hu, X.; Liu, C.; Sun, Y.; Hou, J.; Li, Y.; Zheng, J.; Chuang, S.; Karim, A.; Gong, X. Enhanced Performance of Polymer Solar Cells Using PEDOT:PSS Doped with $Fe_3O_4$ Magnetic Nanoparticles Aligned by an External Magnetostatic Field as an Anode Buffer Layer. *ACS Appl. Mater. Interfaces* **2014**, *6*, 13201−13208.

(15) Thomas, J. P.; Zhao, L.; McGillivray, D.; Leung, K. T. High-Efficiency Hybrid Solar Cells by Nanostructural Modification in PEDOT:PSS with Co-solvent Addition. *J. Mater. Chem. A* **2014**, *2*, 2383−2389.

(16) Kim, Y. H.; Sachse, C.; Machala, M. L.; May, C.; Müller-Meskamp, L.; Leo, K. Highly Conductive PEDOT:PSS Electrode with Optimized Solvent and Thermal Post-Treatment for ITO-Free Organic Solar Cells. *Adv. Funct. Mater.* **2011**, *21*, 1076−1081.

(17) Yeo, J.-S.; Yun, J.-M.; Kim, D.-Y.; Park, S.; Kim, S.-S.; Yoon, M.-H.; Kim, T.-W.; Na, S.-I. Significant Vertical Phase Separation in Solvent-Vapor-Annealed Poly(3,4-ethylenedioxythiophene):Poly(styrene sulfonate) Composite Films Leading to Better Conductivity and Work Function for High-Performance Indium Tin Oxide-Free Optoelectronics. *ACS Appl. Mater. Interfaces* **2012**, *4*, 2551−2560.

(18) Kim, J.; Kim, H.; Kim, G.; Back, H.; Lee, K. Soluble Transition Metal Oxide/Polymeric Acid Composites for Efficient Hole-Transport Layers in Polymer Solar Cells. *ACS Appl. Mater. Interfaces* **2014**, *6*, 951−957.

(19) Chen, J.-G.; Wei, H.-Y.; Ho, K.-C. Using Modified Poly(3,4-ethylene dioxythiophene): Poly(styrene sulfonate) Film as a Counter Electrode in Dye-Sensitized Solar Cells. *Sol. Energy Mater. Sol. Cells* **2007**, *91*, 1472−1477.

(20) Zhang, Z.; Zhang, X.; Xu, H.; Liu, Z.; Pang, S.; Zhou, X.; Dong, S.; Chen, X.; Cui, G. $CuInS_2$ Nanocrystals/PEDOT:PSS Composite Counter Electrode for Dye-Sensitized Solar Cells. *ACS Appl. Mater. Interfaces* **2012**, *4*, 6242−6246.

(21) Xu, H.; Zhang, X.; Zhang, C.; Liu, Z.; Zhou, X.; Pang, S.; Chen, X.; Dong, S.; Zhang, Z.; Zhang, L.; Han, P.; Wang, X.; Cui, G. Nanostructured Titanium Nitride/PEDOT:PSS Composite Films as Counter Electrodes of Dye-Sensitized Solar Cells. *ACS Appl. Mater. Interfaces* **2012**, *4*, 1087−1092.

(22) Yoo, D.; Kim, J.; Kim, J. H. Direct Synthesis of Highly Conductive Poly(3,4-ethylenedioxythiophene):Poly(4-styrenesulfonate) (PEDOT:PSS)/Graphene Composites and Their Applications in Energy Harvesting Systems. *Nano Res.* **2014**, *7*, 717−730.

(23) Zhang, B.; Tan, G.; Lam, C.-S.; Yao, B.; Ho, C.-L.; Liu, L.; Xie, Z.; Wong, W.-Y.; Ding, J.; Wang, L. High-Efficiency Single Emissive Layer White Organic Light-Emitting Diodes based on Solution-Processed Dendritic Host and New Orange-Emitting Iridium Complex. *Adv. Mater.* **2012**, *24*, 1873−1877.

(24) Zhu, Z.-T.; Mabeck, J. T.; Zhu, C.; Cady, N. C.; Batt, C. A.; Malliaras, G. G. A Simple Poly(3,4-ethylene dioxythiophene)/Poly(styrene sulfonic acid) Transistor for Glucose Sensing at Neutral pH. *Chem. Commun.* **2004**, 1556−1557.

(25) Kuş, M.; Okur, S. Electrical Characterization of PEDOT:PSS beyond Humidity Saturation. *Sens. Actuators, B* **2009**, *143*, 177−181.

(26) Crispin, X.; Jakobsson, F. L. E.; Crispin, A.; Grim, P. C. M.; Andersson, P.; Volodin, A.; van Haesendonck, C.; Van der Auweraer, M.; Salaneck, W. R.; Berggren, M. The Origin of the High Conductivity of Poly(3,4-ethylenedioxythiophene)-Poly(styrenesulfonate) (PEDOT-PSS) Plastic Electrodes. *Chem. Mater.* **2006**, *18*, 4354−4360.

(27) Park, H.-S.; Ko, S.-J.; Park, J.-S.; Kim, J. Y.; Song, H.-K. Redox-Active Charge Carriers of Conducting Polymers as a Tuner of Conductivity and Its Potential Window. *Sci. Rep.* **2013**, *3*, 2454.

(28) Jönsson, S. K. M.; Birgerson, J.; Crispin, X.; Greczynski, G.; Osikowicz, W.; van der Gon, A. W. D.; Salaneck, W. R.; Fahlman, M. The Effects of Solvents on the Morphology and Sheet Resistance in Poly(3,4-ethylenedioxythiophene)−Polystyrenesulfonic Acid (PEDOT−PSS) Films. *Synth. Met.* **2003**, *139*, 1−10.

(29) Huang, L.-M.; Lin, H.-Z.; Wen, T.-C.; Gopalan, A. Highly Dispersed Hydrous Ruthenium Oxide in Poly(3,4-ethylenedioxythiophene)-Poly(styrene sulfonic acid) for Supercapacitor Electrode. *Electrochim. Acta* **2006**, *52*, 1058−1063.

(30) Sellam; Hashmi, S. A. High Rate Performance of Flexible Pseudocapacitors Fabricated Using Ionic-Liquid-Based Proton Conducting Polymer Electrolyte with Poly(3,4-ethylenedioxythiophene):Poly(styrene sulfonate) and Its Hydrous Ruthenium Oxide Composite Electrodes. *ACS Appl. Mater. Interfaces* **2013**, *5*, 3875−3883.

(31) Chen, L.; Yuan, C.; Dou, H.; Gao, B.; Chen, S.; Zhang, X. Synthesis and Electrochemical Capacitance of Core−Shell Poly (3,4-ethylenedioxythiophene)/Poly (sodium 4-styrenesulfonate)-Modified Multiwalled Carbon Nanotube Nanocomposites. *Electrochim. Acta* **2009**, *54*, 2335−2341.

(32) Chu, C.-Y.; Tsai, J.-T.; Sun, C.-L. Synthesis of PEDOT-Modified Graphene Composite Materials as Flexible Electrodes for




DOI: 10.1021/acsami.5b00657
*ACS Appl. Mater. Interfaces* 2015, 7, 10213−10227

Energy Storage and Conversion Applications. *Int. J. Hydrogen Energy* **2012**, *37*, 13880−13886.
(33) Yang, Y.; Li, S.; Zhang, L.; Xu, J.; Yang, W.; Jiang, Y. Vapor Phase Polymerization Deposition of Conducting Polymer/Graphene Nanocomposites as High Performance Electrode Materials. *ACS Appl. Mater. Interfaces* **2013**, *5*, 4350−4355.
(34) Österholm, A. M.; Shen, D. E.; Dyer, A. L.; Reynolds, J. R. Optimization of PEDOT Films in Ionic Liquid Supercapacitors: Demonstration as a Power Source for Polymer Electrochromic Devices. *ACS Appl. Mater. Interfaces* **2013**, *5*, 13432−13440.
(35) Novák, P.; Müller, K.; Santhanam, K. S. V.; Haas, O. Electrochemically Active Polymers for Rechargeable Batteries. *Chem. Rev.* **1997**, *97*, 207−282.
(36) Xu, J.; Schwab, M. G.; Strudwick, A. J.; Henning, I.; Feng, X.; Wu, Z.; Müllen, K. Screen-Printable Thin Film Supercapacitor Device Utilizing Graphene/Polyaniline Inks. *Adv. Energy Mater.* **2013**, *3*, 1035−1040.
(37) Krebs, F. C. Polymer Solar Cell Modules Prepared Using Roll-to-Roll Methods: Knife-Over-Edge Coating, Slot-Die Coating and Screen Printing. *Sol. Energy Mater. Sol. Cells* **2009**, *93*, 465−475.
(38) Kim, G. H.; Hwang, D. H.; Woo, S. I. Thermoelectric Properties of Nanocomposite Thin Films Prepared with Poly(3,4-ethylenedioxythiophene) Poly(styrenesulfonate) and Graphene. *Phys. Chem. Chem. Phys.* **2012**, *14*, 3530−3536.
(39) Stankovich, S.; Piner, R. D.; Chen, X.; Wu, N.; Nguyen, S. T.; Ruoff, R. S. Stable Aqueous Dispersions of Graphitic Nanoplatelets via the Reduction of Exfoliated Graphite Oxide in the Presence of Poly(sodium 4-styrenesulfonate). *J. Mater. Chem.* **2006**, *16*, 155−158.
(40) Stöcker, T.; Köhler, A.; Moos, R. Why Does the Electrical Conductivity in PEDOT:PSS Decrease with PSS Content? A Study Combining Thermoelectric Measurements with Impedance Spectroscopy. *J. Polym. Sci.* **2012**, *50*, 976−983.
(41) Georgakilas, V.; Otyepka, M.; Bourlinos, A. B.; Chandra, V.; Kim, N.; Kemp, K. C.; Hobza, P.; Zboril, R.; Kim, K. S. Functionalization of Graphene: Covalent and Non-Covalent Approaches, Derivatives and Applications. *Chem. Rev.* **2012**, *112*, 6156−6214.
(42) Zhang, J.; Zhao, X. S. Conducting Polymers Directly Coated on Reduced Graphene Oxide Sheets as High-Performance Supercapacitor Electrodes. *J. Phys. Chem. C* **2012**, *116*, 5420−5426.
(43) Yan, X.; Chen, J.; Yang, J.; Xue, Q.; Miele, P. Fabrication of Free-Standing, Electrochemically Active, and Biocompatible Graphene Oxide-Polyaniline and Graphene-Polyaniline Hybrid Papers. *ACS Appl. Mater. Interfaces* **2010**, *2*, 2521−2529.
(44) Liu, P.-B.; Huang, Y.; Sun, X. Excellent Electromagnetic Absorption Properties of Poly(3,4-ethylenedioxythiophene)-Reduced Graphene Oxide−$Co_3O_4$ Composites Prepared by a Hydrothermal Method. *ACS Appl. Mater. Interfaces* **2013**, *5*, 12355−12360.
(45) Liu, S.; Tian, J.; Wang, L.; Luo, Y.; Sun, X. Production of Stable Aqueous Dispersion of Poly(3,4-ethylenedioxythiophene) Nanorods Using Graphene Oxide as a Stabilizing Agent and Their Application for Nitrite Detection. *Analyst* **2011**, *136*, 4898−4902.
(46) Wu, Z.-S.; Wang, D.-W.; Ren, W.; Zhao, J.; Zhou, G.; Li, F.; Cheng, H.-M. Anchoring Hydrous $RuO_2$ on Graphene Sheets for High-Performance Electrochemical Capacitors. *Adv. Funct. Mater.* **2010**, *20*, 3595−3602.
(47) Chang, K.-H.; Hu, C.-C. Hydrothermal Synthesis of Hydrous Crystalline $RuO_2$ Nanoparticles for Supercapacitors. *Electrochem. Solid-State Lett.* **2004**, *7*, A466−A469.
(48) Hansen, C. M. *Hansen Solubility Parameters: A User's Handbook*, 2nd ed.; CRC Press: Boca Raton, FL, 2007.
(49) Park, S.; An, J.; Jung, I.; Piner, R. D.; An, S. J.; Li, X.; Velamakanni, A.; Ruoff, R. S. Colloidal Suspensions of Highly Reduced Graphene Oxide in a Wide Variety of Organic Solvents. *Nano Lett.* **2009**, *9*, 1593−1597.
(50) Thomas, J. D. Chemistry of 2,2′-Azobisisobutyramidine Hydrochloride in Aqueous Solution: a Water-Soluble Azo Initiator. *J. Am. Chem. Soc.* **1961**, *83*, 4849−4853.
(51) Zhou, J.; Lubineau, G. Improving Electrical Conductivity in Polycarbonate Nanocomposites Using Highly Conductive PEDOT/PSS Coated MWCNTs. *Adv. Funct. Mater. Interfaces* **2013**, *5*, 6189−6200.
(52) Skotheim, T. A.; Elsenbaumer, R. L.; Shacklette, L. W. *Handbook of Conducting polymers*, 2nd ed.; Marcel Dekker, Inc.: New York, 1997.
(53) Marina, S.-B.; Kelley, A. M. Surface-Enhanced Raman Study of the Interaction of PEDOT:PSS with Plasmonically Active Nanoparticles. *J. Phys. Chem. C* **2010**, *114*, 6822−6830.
(54) Zhang, X.; Chang, D.; Liu, J.; Luo, Y. Conducting Polymer Aerogels from Supercritical $CO_2$ Drying PEDOT-PSS Hydrogels. *J. Mater. Chem.* **2010**, *20*, 5080−5085.
(55) Kim, M.; Lee, C.; Jang, J. Fabrication of Highly Flexible, Scalable, and High-Performance Supercapacitors Using Polyaniline/Reduced Graphene Oxide Film with Enhanced Electrical Conductivity and Crystallinity. *Adv. Funct. Mater.* **2014**, *24*, 2489−2499.
(56) Xiong, G.; Meng, C.; Reifenberger, R. G.; Irazoqui, P. P.; Fisher, T. S. A Review of Graphene-Based Electrochemical Microsupercapacitors. *Electroanalysis* **2014**, *26*, 30−51.
(57) Xiong, G.; Meng, C.; Reifenberger, R. G.; Irazoqui, P. P.; Fisher, T. S. Graphitic Petal Electrodes for All-Solid-State Flexible Supercapacitors. *Adv. Energy Mater.* **2014**, *4*, 1300515.
(58) Xu, Y.; Huang, X.; Lin, Z.; Zhong, X.; Huang, Y.; Duan, X. One-Step Strategy to Graphene/$Ni(OH)_2$ Composite Hydrogels as Advanced Three-Dimensional Supercapacitor Electrode Materials. *Nano Res.* **2013**, *6*, 65−76.
(59) Gong, C.; He, Y.; Zhou, J.; Chen, W.; Han, W.; Zhang, Z.; Zhang, P.; Pan, X.; Wang, Z.; Xie, E. Synthesis on Winged Graphene Nanofibers and Their Electrochemical Capacitive Performance. *ACS Appl. Mater. Interfaces* **2014**, *6*, 14844−14850.
(60) Leng, K.; Zhang, F.; Zhang, L.; Zhang, T.; Wu, Y.; Lu, Y.; Huang, Y.; Chen, Y. Graphene-Based Li-Ion Hybrid Supercapacitors with Ultrahigh Performance. *Nano Res.* **2013**, *6*, 581−592.
(61) Gao, H.; Xiao, F.; Ching, C. B.; Duan, H. High-Performance Asymmetric Supercapacitor based on Graphene Hydrogel and Nanostructured $MnO_2$. *ACS Appl. Mater. Interfaces* **2012**, *4*, 2801−2810.
(62) Gao, H.; Xiao, F.; Ching, C. B.; Duan, H. Flexible All-Solid-State Asymmetric Supercapacitors based on Free-Standing Carbon Nanotube/Graphene and $Mn_3O_4$ Nanoparticle/Graphene Paper Electrodes. *ACS Appl. Mater. Interfaces* **2012**, *4*, 7020−7026.
(63) Yang, S.; Song, X.; Zhang, P.; Gao, L. Facile Synthesis of Nitrogen-Doped Graphene−Ultrathin $MnO_2$ Sheet Composites and Their Electrochemical Performances. *ACS Appl. Mater. Interfaces* **2013**, *5*, 3317−3322.
(64) Tang, P.; Han, L.; Zhang, L. Facile Synthesis of Graphite/PEDOT/$MnO_2$ Composites on Commercial Supercapacitor Separator Membranes as Flexible and High-Performance Supercapacitor Electrodes. *ACS Appl. Mater. Interfaces* **2014**, *6*, 10506−10515.
(65) Zhu, X.; Zhang, P.; Xu, S.; Yan, X.; Xue, Q. Free-Standing Three-Dimensional Graphene/Manganese Oxide Hybrids as Binder-Free Electrode Materials for Energy Storage Applications. *ACS Appl. Mater. Interfaces* **2014**, *6*, 11665−11674.
(66) Li, P.; Shi, E.; Yang, Y.; Shang, Y.; Peng, Q.; Wu, S.; Wei, J.; Wang, K.; Zhu, H.; Yuan, Q.; Cao, A.; Wu, D. Carbon Nanotube-Polypyrrole Core-Shell Sponge and Its Application as Highly Compressible Supercapacitor Electrode. *Nano Res.* **2014**, *7*, 209−218.
(67) Du, H.; Jiao, L.; Wang, Q.; Yang, J.; Guo, L.; Si, Y.; Wang, Y.; Yuan, H. Facile Carbonaceous Microsphere Templated Synthesis of $Co_3O_4$ Hollow Spheres and Their Electrochemical Performance in Supercapacitors. *Nano Res.* **2013**, *6*, 87−98.
(68) Porada, S.; Weinstein, L.; Dash, R.; van der Wal, A.; Bryjak, M.; Gogotsi, Y.; Biesheuvel, P. M. Water Desalination Using Capacitive Deionization with Microporous Carbon Electrodes. *ACS Appl. Mater. Interfaces* **2012**, *4*, 1194−1199.
(69) Hu, H.; Zhao, Z.; Wan, W.; Gogotsi, Y.; Qiu, J. Polymer/Graphene Hybrid Aerogel with High Compressibility, Conductivity,


DOI: 10.1021/acsami.5b00657
*ACS Appl. Mater. Interfaces* 2015, 7, 10213−10227

and "Sticky" Superhydrophobicity. *ACS Appl. Mater. Interfaces* **2014**, *6*, 3242−3249.
(70) Hatzell, K. B.; Fan, L.; Beidaghi, M.; Boota, M.; Pomerantseva, E.; Kumbur, E. C.; Gogotsi, Y. Polymer/Graphene Hybrid Aerogel with High Compressibility, Conductivity, and "Sticky" Superhydrophobicity. *ACS Appl. Mater. Interfaces* **2014**, *6*, 8886−8893.
(71) Er, D.; Li, J.; Naguib, M.; Gogotsi, Y.; Shenoy, V. B. $Ti_3C_2$ MXene as a High Capacity Electrode Material for Metal (Li, Na, K, Ca) Ion Batteries. *ACS Appl. Mater. Interfaces* **2014**, *6*, 11173−11179.
(72) Deng, L.; Wang, J.; Zhu, G.; Kang, L.; Hao, Z.; Lei, Z.; Yang, Z.; Liu, Z.-H. $RuO_2$/Graphene Hybrid Material for High Performance Electrochemical Capacitor. *J. Power Sources* **2014**, *248*, 407−415.
(73) Liu, R.; Duay, J.; Lane, T.; Lee, S. Synthesis and Characterization of $RuO_2$/poly(3,4-ethylenedioxythiophene) Composite Nanotubes for Supercapacitors. *Phys. Chem. Chem. Phys.* **2010**, *12*, 4309−4316.
(74) Wang, W.; Lei, W.; Yao, T.; Xia, X.; Huang, W.; Hao, Q.; Wang, X. One-pot Synthesis of Graphene/$SnO_2$/PEDOT Ternary Electrodematerial for Supercapacitors. *Electrochim. Acta* **2013**, *108*, 118−126.
(75) Lei, Z.; Chen, Z.; Zhao, X. S. Growth of Polyaniline on Hollow Carbon Spheres for Enhancing Electrocapacitance. *J. Phys. Chem. C* **2010**, *114*, 19867−19874.
(76) Pandey, G. P.; Rastogi, A. C. Solid-State Supercapacitors Based on Pulse Polymerized Poly(3,4-ethylenedioxythiophene) Electrodes and Ionic Liquid Gel Polymer Electrolyte. *J. Electrochem. Soc.* **2012**, *159*, A1664−A1671.
(77) Soin, N.; Roy, S. S.; Mitra, S. K.; Thundat, T.; McLaughlin, J. A. Nanocrystalline Ruthenium Oxide Dispersed Few Layered Graphene (FLG) Nanoflakes as Supercapacitor Electrodes. *J. Mater. Chem.* **2012**, *22*, 14944−14950.
(78) Ouyang, J.; Chu, C.-W.; Chen, F.-C.; Xu, Q.; Yang, Y. Polymer Optoelectronic Devices with High-Conductivity Poly(3,4-Ethylenedioxythiophene) Anodes. *J. Macromol. Sci., Part A: Pure Appl.Chem.* **2004**, *41*, 1497−1511.
(79) Cruz-Cruz, I.; Reyes-Reyes, M.; Aguilar-Frutis, M. A.; Rodriguez, A. G.; López-Sandovald, R. Study of the effect of DMSO concentration on the thickness of the PSS insulating barrier in PEDOT:PSS thin films. *Synth. Met.* **2010**, *160*, 1501−1506.
(80) Kim, H.; Popov, B. N. Synthesis and Characterization of $MnO_2$-Based Mixed Oxides as Supercapacitors. *J. Electrochem. Soc.* **2003**, *150*, D56−D62.
(81) Liu, X.; Lee, E. K.; Oh, J. H. Graphene-Ruthenium Complex Hybrid Photodetectors with Ultrahigh Photoresponsivity. *Small* **2014**, *10*, 3700−3706.
(82) Jung, S.-M.; Lee, E. K.; Choi, M.; Shin, D.; Jeon, I.-Y.; Seo1, J.-M.; Jeong, H. Y.; Park, N.; Oh, J. H.; Baek, J.-B. Direct Solvothermal Synthesis of B/N-Doped Graphene. *Angew. Chem., Int. Ed.* **2014**, *53*, 2398−2401.
(83) Chang, D. W.; Lee, E. K.; Park, E. Y.; Yu, H.; Choi, H.-J.; Jeon, I.-Y.; Sohn, G.-J.; Shin, D.; Park, N.; Oh, J. H.; Dai, L.; Baek, J.-B. Nitrogen-Doped Graphene Nanoplatelets from Simple Solution Edge-Functionalization for *n*-Type Field-Effect Transistors. *J. Am. Chem. Soc.* **2013**, *135*, 8981−8988.


DOI: 10.1021/acsami.5b00657
*ACS Appl. Mater. Interfaces* 2015, 7, 10213−10227